EVALUATION OF A CLOSE COUPLED SLOTTED ORIFICE, ELECTRICAL IMPEDANCE, AND SWIRL FLOW METERS FOR MULTIPHASE FLOW

A Thesis

by

MUHAMMET CEVIK

Submitted to the Office of Graduate and Professeional Studies of
Texas A&M University
in partial fulfillment of the requirements for the degree of

MASTER OF SCIENCE

Chair of Committee,	Gerald Morrison
Committee Members,	Michael Pate
	Yassin A. Hassan
Head of Department,	Andreas Polycarpou

December 2013

Major Subject: Mechanical Engineering

ABSTRACT

The performance of a coupled slotted orifice and swirl flow meters, and a coupled slotted orifice and an impedance probe flow meter for multiphase flow is evaluated to develop a new multiphase flow meter. The slotted orifice also provides well homogenized flow for several pipe diameters downstream of the plate. This characteristic provides a homogeneous mixture at the inlet of the swirl meter, and impedance probe for gas volume fraction measurement (GVF). In order to evaluate the performance of the designed flow-meters, the GVF and mass flow rate responses are investigated at varying pressures (20, 40, and 60 psi) and water flow rates (30, 40, 50, 60, 70, 80, and 90 GPM). The proper correlations are established to provide high accurate two-phase flow measurement. The new proposed approach provides the GVF measurement with less than 0.017 % error, and the total mass flow rate measurement within error ± 0.38 over the range of 4 to 13 lbm/sec.

I dedicate this work to

The only God, the merciful, and gracious

ACKNOWLEDGEMENTS

I would like to thank my advisor, Dr. Morrison, for his guidance throughout my research. I would also like to thank the rest of my committee, Dr. Michael Pate and Dr. Yassin A. Hassan for their support.

I would like to thank everyone at the TurboLab, especially Abhay Patil and Sahand Pirouzpanah for giving me advice and helping me finish my research.

I also would like to thank BOTAS for financial support throughout my master education.

I thank you my parent and my brothers for all their emotional and financial support and guidance.

TABLE OF CONTENTS

Page

LIST OF FIGURES

Page

LIST OF TABLES

Page

1. INTRODUCTION

Two phase flow metering has been important for many years in a variety of industries, such as in the oil and gas, the chemical, the power generation and the nuclear energy industries [1, 2]. The accurate and low cost measurement of flow rate and quality of mixture are needed for many processes in multiphase flow systems [3].

Many methods provide multiphase flow metering. Using separators is a well-known technique to designate the flow rates of fluids in a two-phase system. In this approach, components of mixture fluids are separated and measured individually by using single phase flow metering equipment such as turbine meter and orifice plate. However, the separators have some weakness [1, 2, and 4].

- large size equipments
- high cost
- deficiency of accuracy because of incomplete separation
- application difficulties in remote areas

Particularly, having a multiphase flow meter that has adequate accuracy, cost effectiveness, and compact design is extremely important for offshore facilities and remote locations to allow monitoring and managing the field, cost saving and optimization problems encouraged many companies to develop new types of multiphase flow metering systems such as FRAMO, TEA, and PECO [5].

Measuring the flow by making the flow homogeneous with phase velocities equal in the flow then measuring flow with single phase flow metering devices, is another approach in multiphase flow metering. This method eliminates separation equipment and associated costs. The compact design multiphase flow meters also provide reduced space and weight and increased capabilities for field managing and monitoring in remote areas. High accuracy of measurement of mixture components provides a significant amount of cost savings. Therefore, a multiphase flow meter with high accuracy is always desired. This capability of flow meter also enhances management and monitoring field, efficiency and safety.

2. LITERATURE REVIEW

2.1. Slotted Orifice Plate

The Slotted orifice plate is a differential pressure (DP) flow meter. Morrison [3] designed the slotted orifice plate to measure two phase flow. He [4] also studied performance of the slotted plate by comparing the standard orifice plate for two phase flow measurement through a pipe. The slotted plate is shown in Figure 2.1. Although the working principle of this plate is the same as with the standard orifice plate, its design is completely different than the standard orifice plate. The orifice plate consists of one large hole in the center; on the other hand the slotted plate is made of uniformly distributed rectangular slots in a circular array of pipe across section. This plate is designed to decrease influences of upstream flow obstruction over pressure differences occurred across the plate.

Figure 2.1 Slotted Orifice Flow Meter, β=0.476.

The main advantages of the slotted orifice plate as a differential pressure device;

- Compact design
- Inexpensive
- No moving parts
- Low maintenance
- Wide application range
- Practical instrumentation
- High accuracy.

Macek [8], under advisement of Dr. Morrison, studied the influence plate thickness in 2" pipe and reported that the 0.235" thickness plate provides better wall pressure distributions, and lower pressure drop than the 0.118" thickness plate . He also stated that the slotted plate provides quicker pressure recovery than the standard orifice plate. The main advantages of the slotted orifice plate compare to the standard orifice plate;

- occurrence of the pressure recovery in a short period of time
- a lower overall head loss
- independent of upstream flow conditions
- consistent and well distributed pipe -wall pressure

Morrison [4] also reported superior performance of the slotted plate by comparing a standard orifice plate. The sensitivity of the slotted plate for upstream velocity is less than the standard orifice plate. The variation of discharge coefficient of the orifice plate is from -1% to 6%, area range of flow conditions while the coefficient of the slotted plate is within 0.25% [4, 7].

Ihfe [9], under the direction of Dr. Morrison, investigated the slotted orifice plate behavior as a flow conditioner. It is reported that the slotted plate has superior performance as a flow conditioner compare to tube bundle.

Terracina [10], under the supervision of Dr. Morrison, studied the experimental and numerical development of the slotted plate, and its design parameter. The optimum ratio of plate thickness and slot width was defined to be 0.25 for ideal performance. The rotation of slotted plate within the flanges does not affect pressure drop and meter calibration. The expansion factor, Y, is a very important parameter for the calibration the slotted plate.

Brewer [6], along with Dr. Morrison, investigated the performances of the slotted plate within the 0.5 to 0.43 beta ratio range. The beta ratio (β) is described by ratio of area of the slotted plate to entire cross section of the pipe.

$$\beta = \sqrt{\frac{A_{slots}}{A_{pipe}}} \tag{2.1}$$

The influences of horizontal and vertical setup, compressibility and placement of the differential pressure taps are also investigated. The slotted plate has the ability to shorten pressure recovery distance. After one pipe diameter, pressure recovers even though occurrence of pressure recovery for standard orifice plate takes place at 3.5 D. They reported that the pressure taps must be placed 1D or 2.5D away from upstream and downstream of the slotted plate to obtain accurate results [6].

Flores [11] ,under advisement of Dr. Morrison, evaluated reproducibility between water -air mixture, and water-steam mixture repeatability for the beta ratios of 0.430, 0.467, and 0.500, and the slotted plates that are made from brass and stainless

steel. It was found that these aspects are unaffiliated with Reynolds number of working fluids.

The calibration coefficient for the slotted plate to measure the mass flow rate of mixture is defined as;

$$KY = \frac{4\dot{m}}{\pi d^2 \sqrt{2\ \rho \Delta P}} \tag{2.2}$$

K is the flow coefficient, Y is the expansion factor, ṁ is the mass flow rate, d is the effective diameter (βxD), D is the pipe inner diameter, β is the beta ratio, ρ is the density of the fluid mixture, and ΔP is pressure differences across the slotted plate [3].

Sparks [12], under the direction of Dr. Morrison, also stated that the slotted plate has superior homogenizer performance than the standard orifice plate and V-cone. The slotted plate provides well homogenized down stream flow. The standard orifice plate failed to provide the same performance with the slotted plate. The homogenizer performance of the V-cone even failed to reach the homogenizer performance of standard orifice plate.

2.2. Swirl Flow Meter

The swirl (vortex) flow meter is a density/velocity sensitive device. Because of reliability, high accuracy, wide flow rate scale and stationary parts, the swirl meter has become one of the dominant devices in natural gas measurement [13].

The flow meter contains initially fixed swirl blades, a throat then an expansion cone that is similar to a venturi, end parts are respectively the vortex motion sensor (the piezoelectric sensors) and the de-swirl blades. The fixed swirl shaped blades change the pressure distribution, and this enforces the flow profile to transform from axial into a rotational movement. Because of the venturi body structure, the flow expands, and back flow advances the vortex to precession motion. The helical path creates pressure – velocity variations. Figure 2.2 shows a sketch of a swirl-meter. The piezoelectric sensor perceives those variations. The frequency (*f*) that is provided from the piezoelectric sensor corresponds with volumetric flow rate [13].

Goujon [14] studied the linearity of the vortex meter. The viscosity of fluid has a strong effect on the linearity of vortex meter when the Reynolds number is less than 30 000.The swirl flow meter might not provide accurate results when low pressure gas is used as an operating fluid. He also described the optimum working conditions for the swirl (vortex) flow meter;

- clean liquids
- high pressure gases and vapors
- not high viscosity liquids

Sun [15] investigated an independent study from Goujon [14] to measure the pressure fluctuation for two-phase flow in a vortex flow meter. It is given that the frequency of the pressure variation shows linearity with Reynolds number for 18% GVF range, and the mean amplitude of the pressure fluctuation reduces with GVF. It is also

stated that under the same GVF, the mean amplitude increases when water flow rates increases.

$$\dot{Q} = \frac{f}{K} \tag{2.3}$$

K is a determined value by conducting test and it does not associate with fluid properties, ṁ is mass flow rate, *f* is frequency within ranges of 10 to 1500Hz, ρ is density [16].

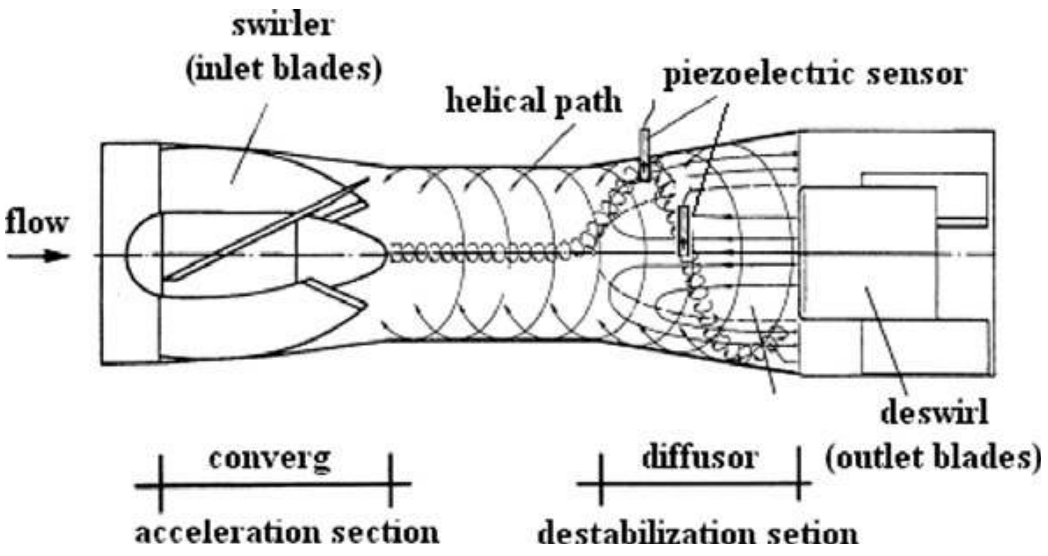

Figure 2.2 A Sketch Of A Swirl-Meter [16].

The main advantages of the swirl (vortex)-meter as a flow meter [17];

- K- factor is independent of fluid properties
- Short required application length for upstream and downstream (3D for upstream, and 1D for downstream)
- easy control over electronic part
- highly accurate metering single phase flow
- contains only stagnant parts
- wide application range

The main disadvantages of the swirl (vortex)-meter as a flow meter [17];

- large size
- high pressure drop
- size dependence at operating flow range

Huga [16] studied the swirl flow meter working behavior under wet gas flow conditions. It is also stated that higher than 90% GVF, the swirl –slotted plated combination can be adequate to use. However, the flow meter is not working well when the vortex precession vanishes which is relative liquid fraction is bigger than 0.12. The gas mass flow rate in the mixture is measured within 6% errors.

Sun [18] investigated swirl flow meter behavior under gas liquid bubble flow conditions. It is reported that within 0-30% gas volume fraction (GVF), the frequency associates with two-phase Reynolds number and flow meter can be used. The swirl

(vortex) flow meter can be used to measure the mass flow rate mixture and GVF can be measure by obtaining frequency, and amplitude with proper correlation. He also stated that the measurement error ±5%.

2.3. Electrical Impedance

The electrical impedance is a widely used method in multiphase measurement. It is very convenient to use for industrial and experimental implementations. The working principle of this technique is that detecting the capacitance and conductivity of a mixture based on fluid type by using more than single electrode mounted on the proper place to the test section [13].

Uga [19] studied the determination of bubble–size distribution with electrical impedance probes. It is given that the electrical impedance probe method is effective to measure bubble behavior and GVF.

Andreussi [20] investigated and designed an electrical impedance measurement device for two phase flow conditions. Two ringed electrodes were used to determine the capacitance or the conductance based on distance between the two electrodes and the amount of liquid which occupied the space between them. The impedance is linearly dependent on the amount of liquid hold-up. When a flow pattern is bubbly flow, the impedance perfectly associated with Maxwell's equation. It is also stated that the impedance method is a very effective way for multiphase flow metering to avoid misreading, it is suggested to keep the distance between electrodes within 1.5 to 2.5 pipe diameter.

Fossa [21] evaluated the performance of the conductance probes for measuring the liquid fraction in multiphase flow. The designed conductance probes show good results to define the phase distribution of mixture. The ring shape and plate electrodes were used for different experimental setups. The electrodes were operated under annular, bubble, and stratified flow profiles. The ring-shaped electrodes showed higher performance than the plate electrodes.

Devia [22] conducted an experiment to design and to optimize the impedance probes for measuring GVF. The ring-shaped and half ring-shaped probes were investigated with geometrical parameters. It is stated that the optimum probes shapes can be produced by considering GVF variations. The half ring shaped probes showed superior results for measuring GVF than the ring- shaped.

Munholand [23] investigated four different probes to determine the most sufficient probe size for measuring local gas friction and bubble velocity. Even though, the classical theory supports that the best results should be obtained from the smallest probe, it is stated that the biggest probe is the most effective and reliable probe.

Da Silva [24] provided the evaluation of the needle probe for multiphase measurement. It is presented that the sensor shows reproducibility, good accuracy, and linearity. The impedance probes can distinguish each phase inside of the multiphase flow from permittivity and conductivity signals. The sensors can also evaluate the concentration of individual components in multiphase flow.

Ismail [25] presented the review of the electrical based methods for two phase flow measurements. It was stated that the impedance associates with the phase distributions and dielectric characteristic of the multiphase, the sizes of electrodes and distance between electrodes.

3. OBJECTIVES

This thesis focuses in six objectives to design an accurate, compact and inexpensive two-phase flow meter:

- To obtain the KY for high accurate the mixture mass flow rate measurements by using the slotted orifice plate and DP.
- To obtain GVF from 100% gas to pure water by using electrical impedance or swirl-meter.
- To obtain the mass flow rate of gas and liquid components in the mixture.
- To determine the optimum position of electrical impedance probes.
- To determine the optimum working frequency of the electrical impedance probes.
- To determine working conditions swirl-meter and electrical impedance for accurate measurement.

4. THEORY

4.1. Ideal Gas Law

The ideal gas law can be used to define gas properties. The equation (4.1) shows that the pressure of gas and the temperature of gas associates with its density.

$$P = \rho_g * R * T \tag{4.1}$$

The density of gas is only dependent on pressure when the temperature is kept constant. Although the pressure variations causes density changes in gas, the density of liquid stay constant at different pressures.

4.2. Mass Flow Rate Of Air

The mass flow rate is the important parameter in measuring process. Mass flow rate of air at the inlet condition is calculated by gathering air density from ideal gas equation, and the volumetric flow rate of air (Q) from a turbine meter.

$$\rho_{air} = \frac{P_{air}}{RT_{air}} \tag{4.2}$$

$$\dot{m}_{air} = \rho_{air}\dot{Q}_{air} \tag{4.3}$$

4.3. The Quality

The quality is used in multiphase flow measurements. ṁ can be used to define the components of fluid , then summed to define total mass flow rate .The quality is proportion of mass flow rate of air to total mass flow rate.

$$X = \frac{\dot{m}_{air}}{\dot{m}_{air} + \dot{m}_{water}} \tag{4.4}$$

4.4. The Gas Volume Fraction

The gas volume friction (GVF) is used in multiphase flow measurements. $\dot{Q}$can be used to define the components of fluid , then summed to define total volumetric flow rate .The gas volume friction is defined as proportion of volumetric flow rate of air to total volumetric flow rate.

$$GVF = \frac{Q_{air}}{Q_{total}} \tag{4.5}$$

4.5. The Mixture Density

The mixture density is also used in multiphase flow. The mixture density is dependent on the density of gas, the density of liquid, and the quality of mixture. The mixture density is determined by using following equation.

$$\rho_{mix} = \frac{\rho_{air}\rho_{water}}{(1-X)\rho_{air} + X\rho_{water}} \tag{4.6}$$

4.6. The Superficial Velocity

The superficial velocity represents the individual velocity of each fluid component in multiphase flow. It is used for defining flow profile. It is dependent on the mass flow rate, the density and, the diameter of pipe. The superficial velocity is defined by using the following equations.

$$U_{sa} = \frac{4\dot{m}_{air}}{\pi D^2 \rho_{air}} \quad (4.7)$$

$\dot{m}_{air}$ is the mass flow rate of air, ρ_{air} is air density, D is pipe inner diameter, U_{sa} is superficial air velocity.

$$U_{sw} = \frac{4\dot{m}_{water}}{\pi D^2 \rho_{water}} \quad (4.8)$$

$\dot{m}_{water}$ is the mass flow rate of water, ρ_{water} is water density, D is pipe inner diameter, U_{sw} is superficial water velocity.

4.7. Beta Ratio

The classical definition of beta ratio is the proportion of orifice area of the orifice plate to the cross section area of pipe. However, in this work, beta ratio is based upon the ratio of area of slots to the cross section area of pipe.

$$\beta = \sqrt{\frac{A_{slots}}{A_{pipe}}} \quad (4.9)$$

4.8. The Calibration Factor (KY)

The calibration factor is used for determination of the slotted plate performance. There are some assumptions are used for calculating the calibration factor.

-Steady state flow

-Incompressible flow $(\rho_{slot} = \rho_{pipe} = \rho)$

The Bernoulli's equation

$$\frac{P_{slot}}{\rho_{slot}} + \frac{{V_{slot}}^2}{2} = \frac{P_{pipe}}{\rho_{pipe}} + \frac{{V_{pipe}}^2}{2} \tag{4.10}$$

The conservation of mass

$$\rho_{slot} A_{slot} V_{slot} = \rho_{pipe} A_{pipe} V_{pipe} \tag{4.11}$$

The fluid velocity of in the slot;

$$V_{slot} = \sqrt{\frac{2(P_{pipe} - P_{slot})}{\rho\left(1 - \frac{A_{slot}}{A_{pipe}}\right)^2}} \tag{4.12}$$

The pressure differences of upstream and downstream;

$$\Delta P = P_{upstream} - P_{sdownstream} \tag{4.13}$$

The theoretical total mass flow rate;

$$\dot{m}_{th} = \frac{A_{slots}}{\sqrt{1 - \left(\frac{A_{slots}}{A_{pipe}}\right)^2}} \sqrt{2\rho\Delta P} \tag{4.14}$$

The actual total mass flow rate is calculated using an empirical coefficient and the theoretical total mass flow rate.

$$\dot{m}_{ac} = C\dot{m}_{th} \tag{4.15}$$

When actual mass flow rate is given by;

$$\dot{m}_{ac} = C \frac{A_{slot}}{\sqrt{1-\beta^4}} \sqrt{2\rho\Delta P} \tag{4.16}$$

The incompressibility assumption should be considered when the flow consists of compressible gas. That is why the expansion factor (Y) is added the equation for accurate calculation of total mass flow rate.

$$\dot{m}_{ac} = CY \frac{\pi(\beta D_{pipe})}{4\sqrt{1-\beta^4}} \sqrt{2\rho\Delta P} \tag{4.17}$$

The K coefficient is derived from C and β by using following equation.

$$K = \frac{C}{\sqrt{1-\beta^4}} \tag{4.18}$$

Then KY, the calibration factor is derived from the following equation.

$$KY = \frac{4\dot{m}_{ac}}{\pi(\beta D_{pipe})^2 \sqrt{2\rho\Delta P}} \tag{4.19}$$

5. EXPERIMENTAL FACILITY

This chapter presents all required experimental equipment to produce data for two-phase flow measurement at the Turbomachinery Laboratory of Texas A&M University. The description of the experimental hardware, the test section, the instrumentation, and data acquisition are given.

5.1. Experimental Hardware

This section will present how air and water are stored and transported. The water flow is provided by using a 100 GPM centrifugal pump from a 5000 gallon storage tank. Two electro-pneumatic valves which are mounted before turbine flow meters provide control of the water flow. The water volumetric flow rate is measured based on operating ranges by two turbine flow meters which are calibrated for water as GPM. A series of oil free air compressors supply pressured air to the test section. The air flow is also controlled by an electro-pneumatic valve which placed after two turbine meters. Turbine meters are calibrated for air, and they measures volumetric flow of air as ACFM. After the air and water are brought to the test section separately, and are mixed at 10 inches away from the inlet of the test section. The water will return the water storage after passing through the test section, and air is released to the atmosphere. Figure 5.1 and Figure 5.2 present water operating system outside of laboratory. 100 GPM centrifugal water pump provides water directly to water controlled units inside of the laboratory.

Figure 5.1 Water Reservoir.

Figure 5.2 Centrifugal Pump And Pressure Regulator.

The Figure 5.3 presents the water control units inside of the laboratory. A PID controller in LabVIEW is used to control the electro-pneumatic valves. The control valves are used to obtain desired water flow, and flow meters measure the flow.

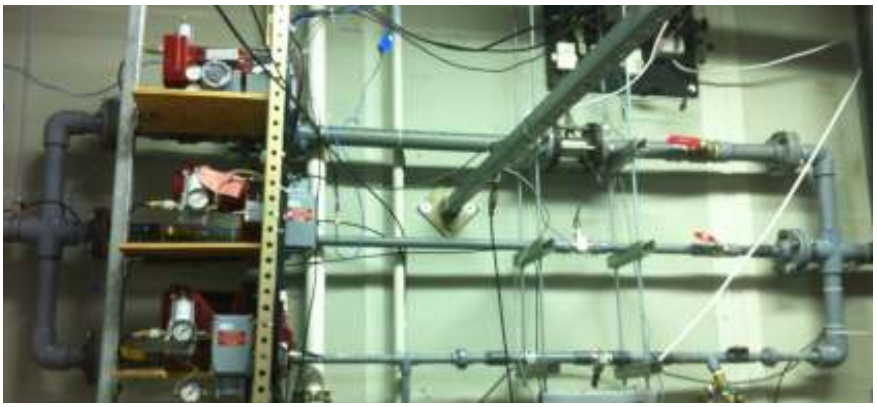

Figure 5.3 Water Manifold.

Air control units are presented by Figure 5.4 and Figure5.5. The oil free compressors supply 100 psi pressurized air to the system. The air control unit inside of laboratory provides controlling and measuring air flow. A PID controller in LabVIEW is used to control the electro-pneumatic valves. The electro-pneumatic valves used after the flow meters.

Figure 5.4 Oil-Free Air Compressors.

Figure 5.5 Air Manifold.

Figure 5.6 shows the electro-pneumatic valve mounted at the end of test section. The valve regulates the pressure in to the test section. A PID controller in LabVIEW is used to control the electro-pneumatic valves.

Figure 5.6 Masoneilan Control Valve.

Two thermocouples are used to measure air and water inlet temperature as˚F.

5.2. Test Section

Two different two-phase flow meters are designed in this project. Therefore, two different test sections are designed.

5.2.1. The Test Section Of The Close Coupled Slotted Plate And Swirl-Meter

This two-phase flow meter prototype consists of stainless steel pipe with 2 inch inner diameter, the slotted plate and a swirl flow meter, two pressure transmitters. The Figure 5.7 shows the close coupled slotted plate and swirl-meter. The pressure taps are placed 1D away from slotted plate for upstream and downstream. The ABB (swirl-meter) is placed two diameter of pipe downstream of the slotted plate. This place was chosen because of the hypothesis that the slotted plate provides well homogenize flow which helps to increase accuracy and repeatable results for the ABB meter (swirl-meter),and it also helps to enhance the measurement ranges. The total length of test section is 10D, and there is not any additional equipment or flow conditioner added before 5D of upstream pipe, to obtain accurate results. Hence, the slotted plate has same characteristic a flow conditioner for upstream of flow.

The raw frequency signal extracted from the ABB swirl flow meter as a output for measurement. The frequency was squared wave form. This frequency output was conditioned by Fast Fourier transform (FFT) module in Lab VIEW. The FFT output and the section pressure were used to find correlation to measure GVF.

Figure 5.7 The Close Coupled Slotted Plate And Swirl-Meter.

The air and water are brought to the test section separately, and are mixed at 10 inches away from the inlet of the test section. The water will return the water storage after passing through the test section; air is released to the atmosphere.

5.2.2. The Test Section Of The Close Coupled Slotted Plate And Electrical Impedance Probes

In Initial test section, the slotted orifice plate, two electrical impedance probes, two 2 inch long PVC with 2 inch inner diameter were used. The slotted plate replaced between two PVC. The pressure taps were placed 1D away from slotted plate for upstream and downstream locations. The PVCs were sandwiched along with the slotted

plate between flanges. The probes were located 1 inch away from the slotted plate downstream. Figure 5.8 shows the initial test section for electrical impedance probes.

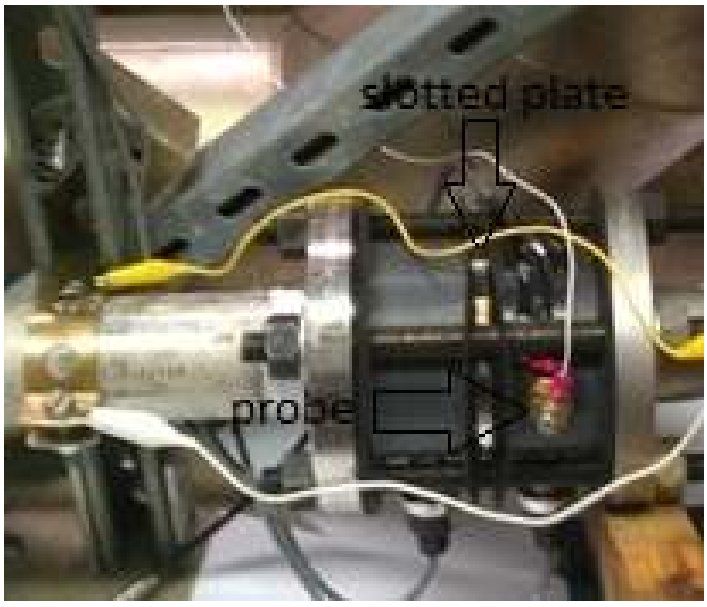

Figure 5.8 The Initial Test Section Of Electrical Impedance Probe.

The secondary test section consists of transparent schedule 80 PVC with 2 inch inner diameter to provide proper visualization to observe the flow profile, the slotted plate and six brass probes, the differential pressure (DP) and the pressure transmitter and the tube bundle. The Figure 5.9 shows the close coupled slotted plate and electrical

impedance. The flow meter can work safely up to 135 psi at room temperature by using 80 PVC. The flanges are not transparent, based on cost conditions.

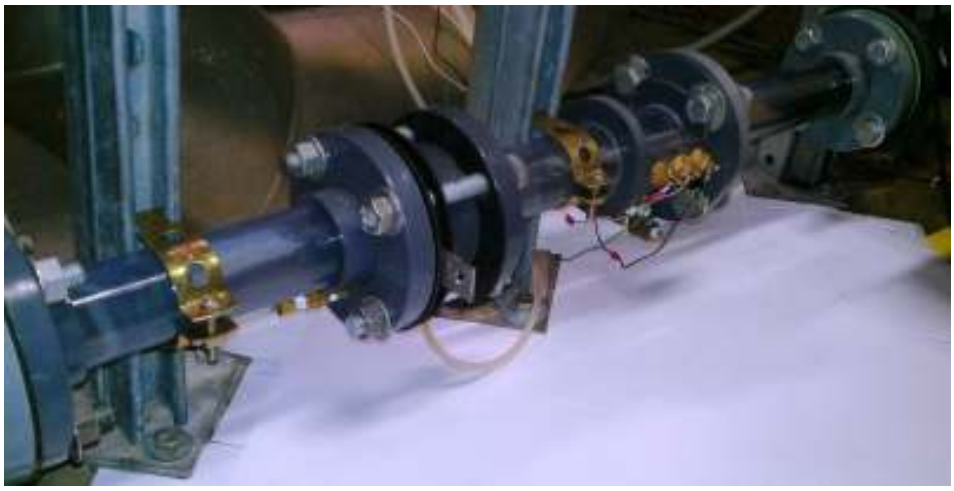

Figure 5.9 The Close Coupled Slotted Plate And Electrical Impedance Probes.

The pressure taps are placed 1D away from slotted plate for upstream and downstream locations. Three different electrical impedance probe position are tested. The two per probes are mounted respectively 10, 11, 12 inch away from the slotted plate and the end of three group probes are flush with the inner wall of pipe. The total length of test section is 15D, and there is not any additional equipment or flow conditioner

added before 5D of upstream pipe, to obtain accurate results. Hence, the slotted plate has same characteristic a flow conditioner for upstream of flow.

The air and water are brought to the test section separately, and are mixed at 10 inches away from the inlet of the test section. The water will return the water storage after passing through the test section; air is released to the atmosphere.

5.3. Instrumentation

To accurately evaluate the two-phase flow meters at variety of GVFs, pressures, and water volumetric flows were used. The pressure transducers, differential pressure transducer, turbine flow meters, thermocouples, the electro-pneumatic valves are used.

5.3.1. Turbine Flow Meters

A turbine flow meter is known as an axial meter. It uses the mechanical motion of the turbine in the fluid flow, which is straightened to reduce turbulence effect. The rotation speed of the turbine associates with the speed of operating fluid. The rotation of turbine generates a signal of AC voltage .This signal is output of the turbine flow meter, and it is associated with flow rate. The turbine flow meter have to placed 10D away from any equipment at upstream ,and 5D away from any equipment at downstream to obtain accurate measurement. Table 5.1 shows the model and range of the turbine meters. Two different range flow meters are used to cover the range air flow rate of 1-130 ACFM. Two different range flow meters are used to measure water flow rate within 5-180 GPM range.

Table 5.1 Flow Meters

Fluid	Range	Model	Range	
Air	High	Omega FTB-938	10-130	ACFM
Air	Low	Omega FTB-933	1-10	ACFM
Water	High	Omega FTB-1425	15-180	GPM
Water	Medium	Omega FTB-1441	5-50	GPM

5.3.2. Pressure Transducers

The Pressure of the downstream of the slotted plate is measured by a Rosemount 2088 pressure transducer. Figure 5.10 shows the Rosemount 2088 pressure transducer used in the experiment. The input voltage of the pressure transducer is 18 VDC, and the output voltage of the pressure transducer is variation 1 to 5 VDC based on pressure changes. The error of the pressure transducers is 0.075 %. The range of the transducer is 0 to 136 psi.

Figure 5.10 A Rosemount 2088 Pressure Transducer.

5.3.3. Differential Pressure Transducer

The measurement the pressure difference is required to calculate the mass flow rate of fluid by using the slotted plate calibration factor (KY). Thus, the pressure difference is measured by a Rosemount 3051 differential pressure transducer. The Figure 5.11 shows a Rosemount 3051 differential pressure transducer used in the experiment. The differential pressure transducer taps are placed 1D away from upstream and downstream of the slotted plate. The output signal of transducer is 4 to 20mA based on pressure variation. The range of differential pressure transducer is 0 to 36 psi. The error of the Rosemount 3051 is 0.065%.

Figure 5.11 A Rosemount 3051 Differential Pressure Transducer.

5.3.4. Thermocouples

Two Omega T-Type thermocouples provide signals for the measurement inlet water and inlet air temperatures. The thermocouples work based on Peltier effect principle. NI-9213 card is used to convert the signal to temperature value as ˚F. The error of Omega T-Type thermocouple is 0.5 F.

5.3.5. Control Valves

Masoneilan Camflex Rotatory Control Valves are used to control the downstream pressure of the slotted plate and the inlet flow rates of air/ water to the test section. The 4-20 mA signals are the output of the valves to obtain desired flow conditions. A PID controller in LabVIEW is used to control the valves. Figure 5.12 shows a Masoneilan Camflex Rotatory Control Valve.

Figure 5.12 A Masoneilan Camflex Rotatory Control Valves.

5.4. Data Acquisition

5.4.1. DAQ Chassis

To measure the flow rates and flow conditions of the operating fluids, different types of sensors, flow meters and control valves are used. These equipments are integrated into an NI-9172 module chassis. The NI-9205 and NI-9215 modules measure pressures from the pressure transducers and differential pressure transducer. The NI-9213 module measures temperatures as ˚F from thermocouples data. The NI-9265 regulates the control valves to reach desired flow conditions. Figure 5.13 shows the NI-9172 module chassis which stores the four NI modules connected to LabVIEW.

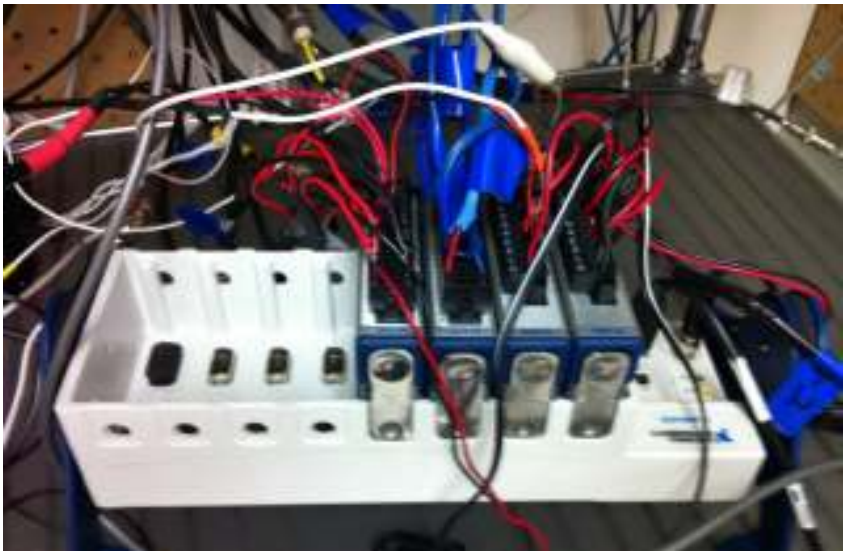

Figure 5.13 A NI-9172 Module Chassis.

5.4.2. NI PCI -611

A stand-alone computer is used to operate the impedance system. Two different cards are used in the computer. The input signal of the electrode is provided by the analog output of a NI PCI -611. The signal consists of ten different frequencies to determine optimum working condition. The working frequency varies from 10 kHz to 4 MHz. The board contains 8 digital I/O lines and two 24-bit counters; analog and digital triggering. Figure 5.14 shows a NI PCI -611.

Figure 5.14 A NI PCI -611.

5.4.3. PCI-DAS4020/12 Analog And Digital I/O Board

PCI-DAS4020/12 analog and digital I/O board is used to measure the output signal which comes from the electrodes. The board is ultra-high–speed multi-function, and it contains 4 analog input channels, 24 digital I/O lines. The Figure5.13 shows a PCI-DAS4020/12 Analog and Digital I/O Board.

5.4.4. LabVIEW

Two different LabVIEW setups are used for two different experimental setups. Figure 5.16 and Figure 5.17 show the LabVIEW programs. The LabVIEW programs have the ability to show all the temperatures, air/water flow rates, GVF, pressures, the input output signals of the electrodes, and the signal which comes from the swirl- meter with short delay. The PIDs controls and regulates the test section pressure, GVF, water

flow rate. The program calculates velocity and GVF by using data which comes from flow meters and pressure transducers.

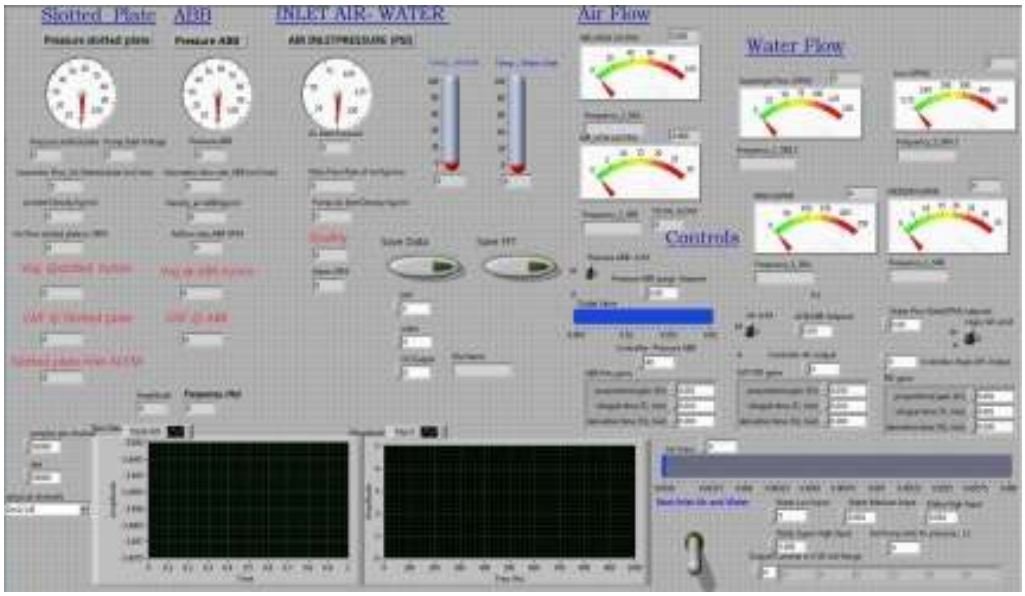

Figure 5.15 LabVIEW Program 1 (The Close Coupled Slotted Plate and the Swirl Meter).

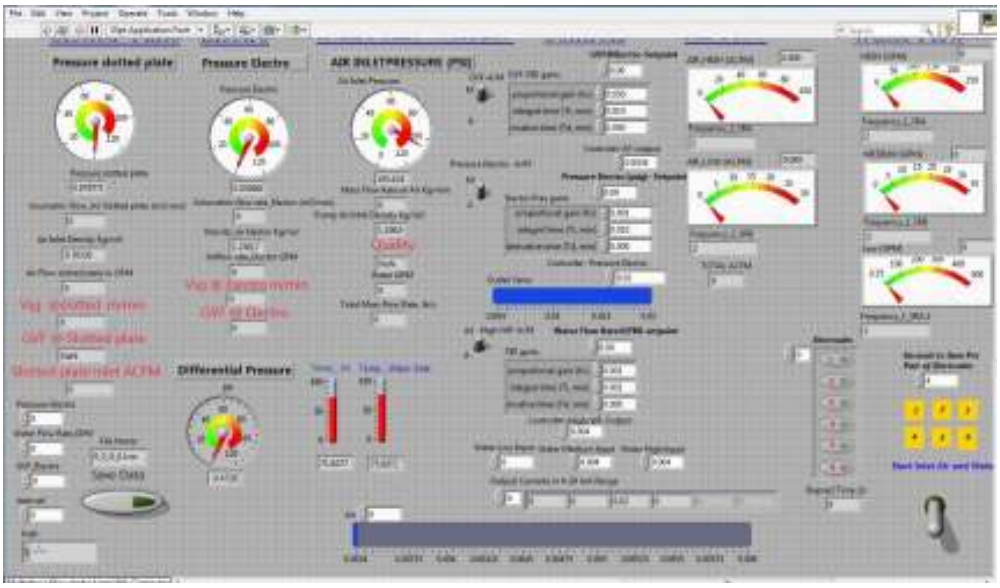

Figure 5.17 Labview Program 2 (The Close Coupled Slotted Plate and the Electrical Impedance Probe).

5.4.5. PID Controller

PID controllers in LabVIEW control the pressure of the test section, the water flow rate inside the test section and GVF of the test section.

5.4.6. GVF And Velocity Calculation

Figure 5.18 shows the real time calculation of both GVF and velocities of water /air. The real time calculation of the GVF and velocity are important to reach desired operating conditions.

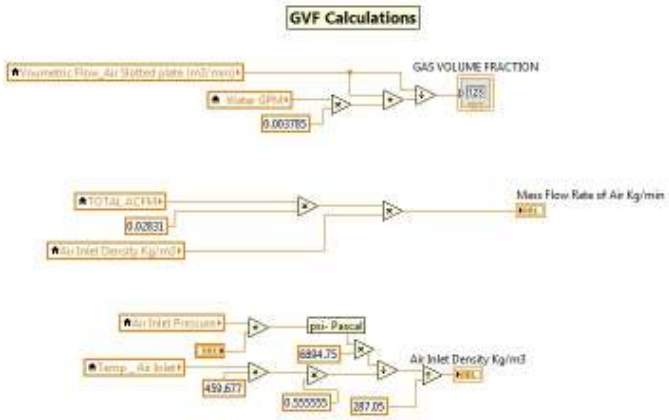

Figure 5.18 GVF And Velocity Calculation.

The density of air is calculated by using air- inlet pressure which is obtained from pressure transducer, and temperature. GVF is calculated volumetric flow rate of water and air which are provided from turbine flow meters.

5.5. Electrical Impedance Probe

The probes are made of ultra-machinable brass. The governing equation is given to determine probe geometry following equation. The Figure 5.19 shows the sensor.

$$C = K\varepsilon_0\varepsilon_r\frac{A}{D} \tag{5.1}$$

C is measured capacitance in system, K is calibration factor for geometry, ε_0 is electrical constant (8.854×10^{-12} F m^{-1}), ε_r is air/water permittivity, A is area of probe, and D is pipe diameter.

The capacitance of the test section (C) was measured when the system was only filled up with water/air. Then K is calculated by using equation 5.1.

Although Devia [22] defined the half ring shaped probe is superior for GVF measurement, the rod type of probes are used based on manufacturing ,cost and operating conditions. The probes geometry factor K is defined 50.

A circuit designed to use between the input and output of the electrodes for high accurate measurement. The Figure 5.20 shows the circuit.

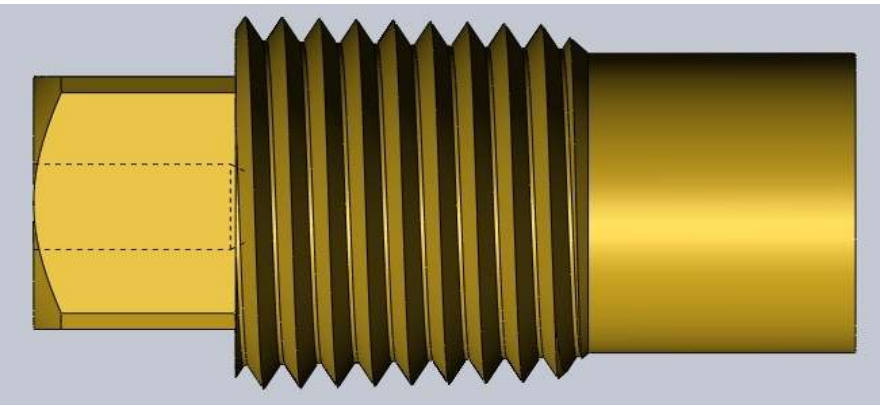

Figure 5.19 The electrical impedance probe.

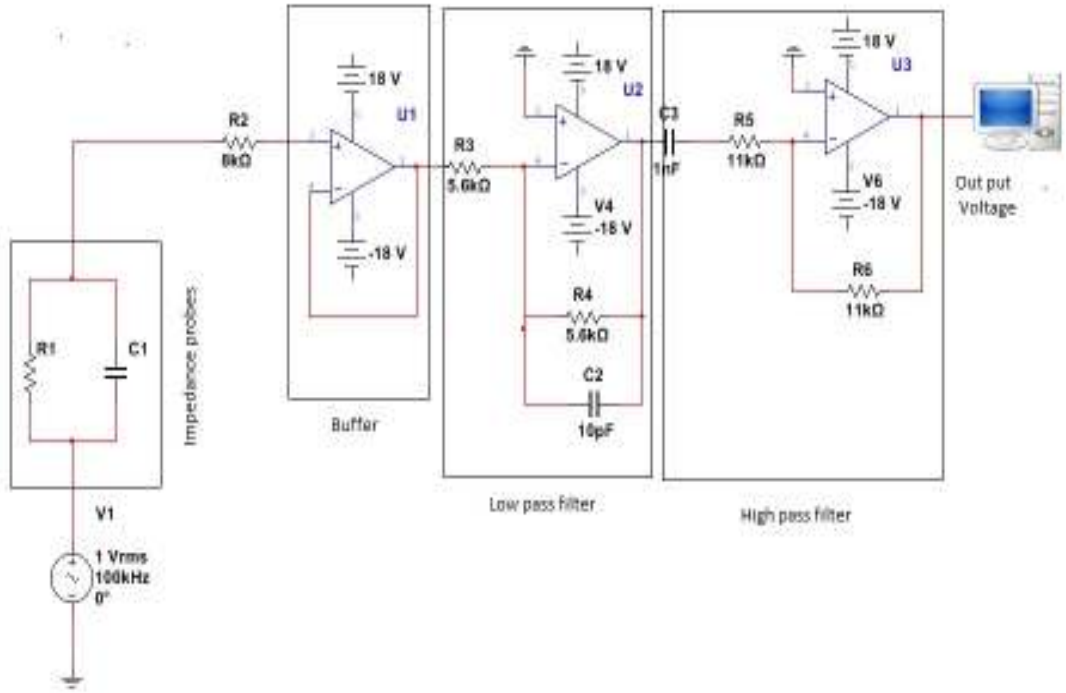

Figure 5.20 The circuit.

6. RESULTS

In this chapter, the results of the evaluation of the close coupled slotted plate and the swirl-meter and the electrical impedance flow meters for multiphase flow are presented.

The results are obtained by setting the pressure of the test section, the GVF of two-phase flow, and the water flow rate. The setting pressures are 20, 40, and 60 psi. The setting water flow rates are 30, 40, 50, 60, 70, 80, and 90 GPM. The setting GVFs are from 10 to 95 %. The optimum working conditions and accuracy of the close coupled slotted plate and the swirl-meter, and the close coupled slotted plate and the electrical impedance flow meters are obtained by testing these conditions.

6.1. The Swirl-Meter

The frequency output of the swirl-meter is repeatable from 60 to 95 % GVF. When the GVF is less than 60 %, frequency loss and too much fluctuation causing misreading are observed. The results show that the frequency associates with GVF and the test section pressure. The gauge pressure, the frequency of swirl-meter, the given GVF are used for adequate curve fitting, and used to obtain a calibration curve GVF (f, P) for the swirl-meter. The standard deviation of fitting is 0.002, and the regression value of the surface (r^2) is 0.9956. Figure 6.1 shows the calibration curve.

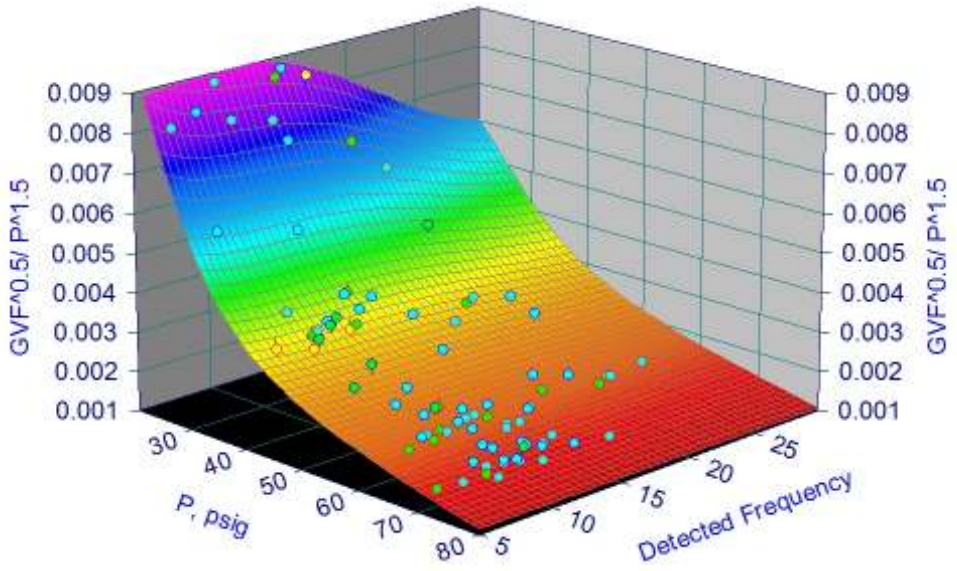

Figure 6.1 The Calibration Curve For The Swirl Meter.

The Figure 6.2 displays the differences of the calculated GVF and measured GVF as a function of GVF. The figure also presents that the standard deviation of the Figure 6.1 does not correspond with Figure 6.2 and thus the relation from Figure 6.1 is not proper to use. However, it can be stated that the swirl-meter output frequency is repeatable for higher than 60%GVF, and the frequency variation associates with GVF and test section pressure. Figure 6.2 also shows that there is an association between the error and GVF.

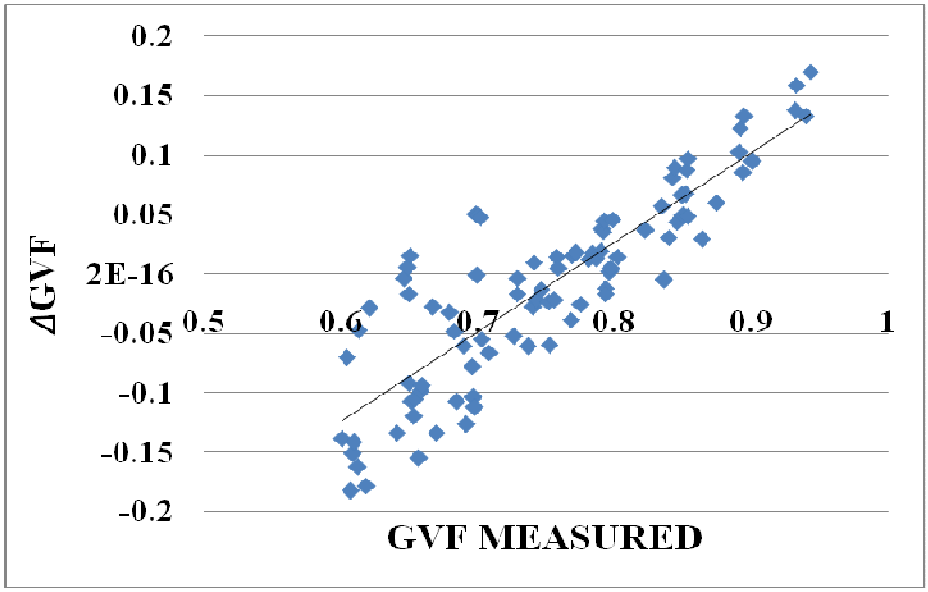

Figure 6.2 The Error of GVF and the Measured GVF for Swirl-Meter (As A Function Of GVF).

Figure 6.2 also shows that the error associates with GVF. Therefore, another curve fitting is prepared to find relation error and measured GVF.

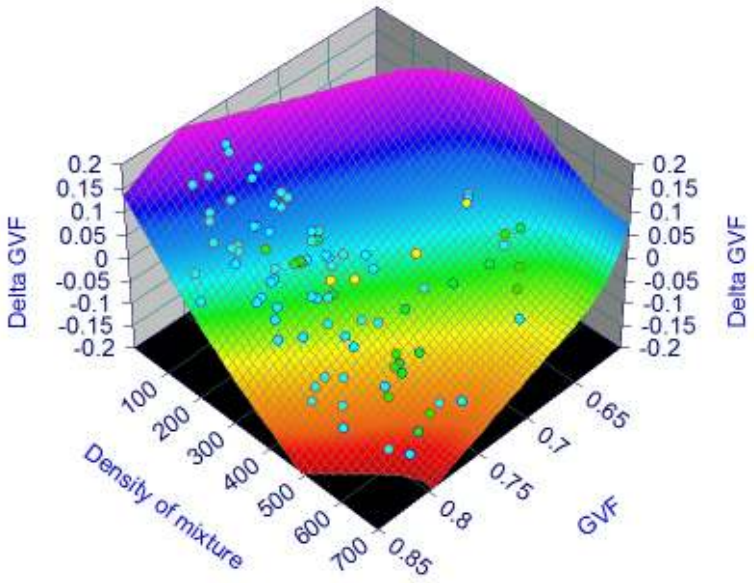

Figure 6.3 The Relation Error, The Measured GVF And The Density Of Mixture.

Figure 6.3 shows the curve fitting for GVF, error and the density of the mixture. The regression value of the surface (r^2) is 0.998, and the standard deviation of fitting is 0.0029.

These two relations are used for iteration to calculate of GVF. Figure 6.4 displays the differences of the calculated GVF and measured GVF as a function of GVF.

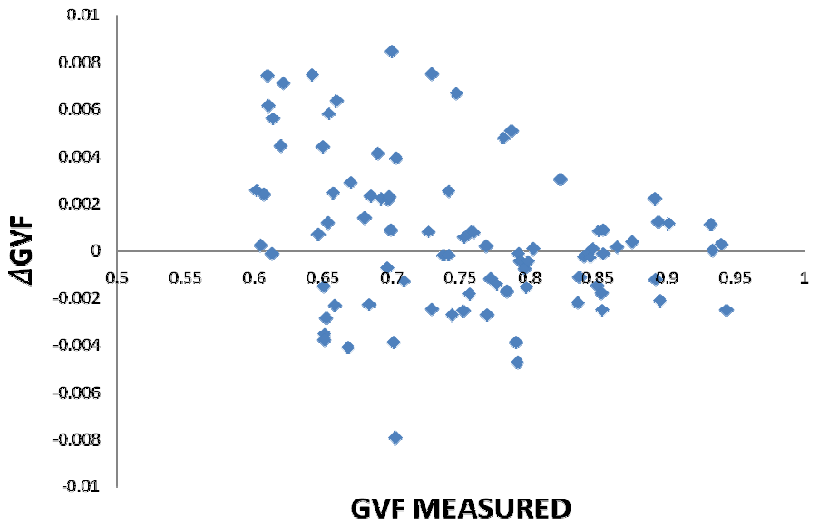

Figure 6.4 The Error Of The GVF And The Measured GVF (As a Function of GVF) After Iteration.

The results show that the pressure of the test section and the density of mixture are important factors to obtain GVF. The output frequency is independent from water and air flow rates and the temperature of mixture. The accurate GVF measurement can be provided from the slotted plate–the swirl meter combination.

6.2. The Electrical Impedance Probe

The electrical impedance probe was used to measure the GVF of the operating mixture in the initial test section along with swirl-meter. Figure 6.5 shows the result of the performance of the electrical impedance probe.

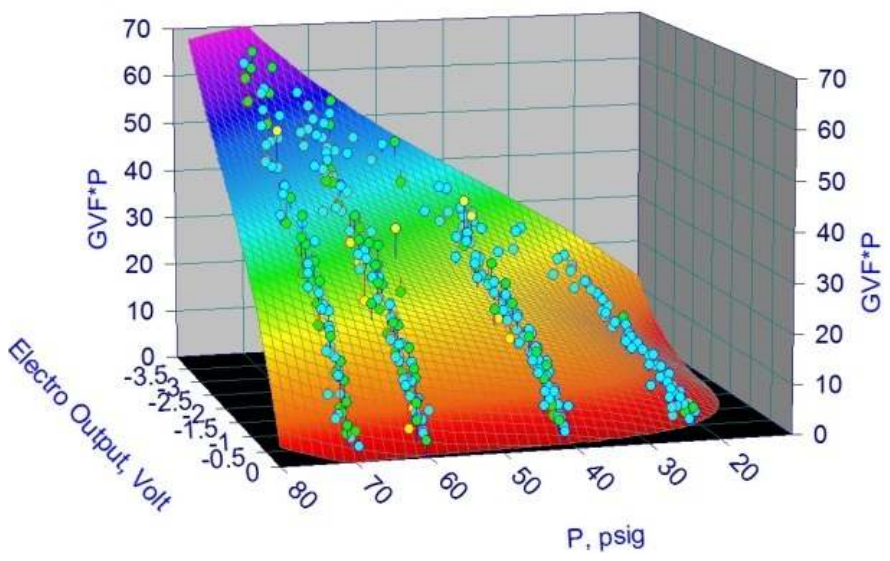

Figure 6.5 The Curve Fitting For Impedance Probe To Measure GVF.

The standard deviation of the curve is 0.04.The result shows that the electrical impedance probe has good performance to measure GVF. Thus, a further investigation is conducted for measuring GVF with only the electrical impedance probe.

The output of the electrical impedance probe shows good response within 10 to 100 % GVF. When the GVF is less than 10 %, the output voltage is low which causes misreading. The results show that the output voltage of the electrical impedance sensor associates with GVF and the temperature of the mixture. The sensor is independent of the variation of the water flow rate and the test section pressure. The temperature, the voltage from the electrical impedance probes, and the given GVF were curve fitted, producing a proper calibration curve {GVF (V, P)}.Ten different frequencies were used

for the input signal of the probe, those frequencies are 13 , 57, 100, 143, 187, 230, 273, 317, 360, and 403 kHz. Six electrical impedance probes were used to find the optimum position. The data was collected from two of the nine different combinations of the six sensors. Figure 6.6 shows the positions of probes. The sensor combinations were provided by selection of the two sensors where one is from left side, and other one from right side. All sensors were marked by position and distance from slotted plate. For position and frequency, the calibrations curves were produced.

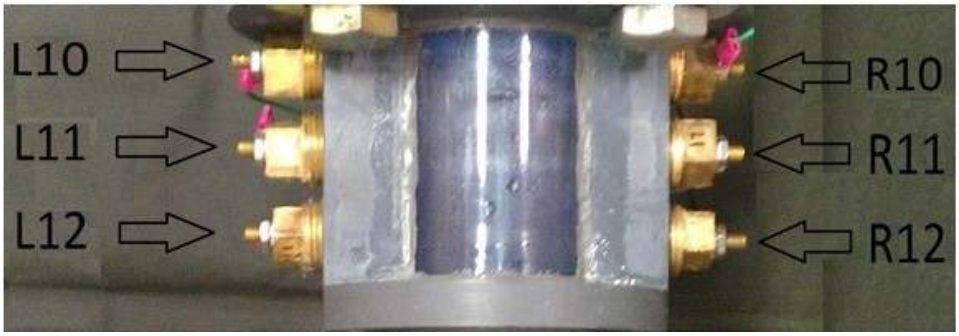

Figure 6.6 The Positions Of Probes.

Figure 6.7 shows the best calibration curve for the electrical impedance probe based on position and frequency. The position is L12-R10, and the frequency is 100 kHz.

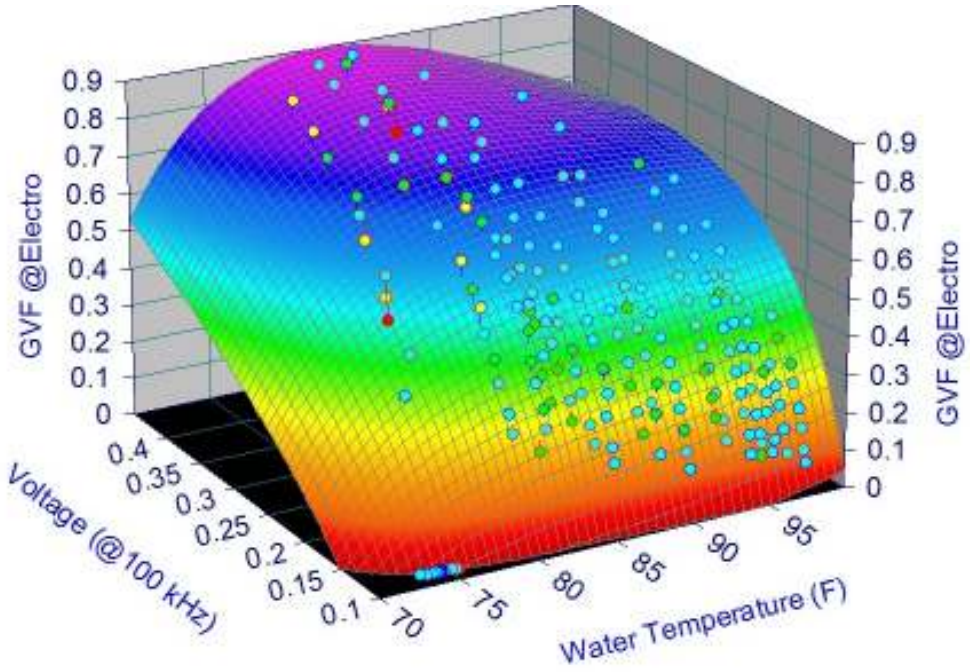

Figure 6.7 The Best Calibration Curve For The Electrical Impedance Probe (Based On Position And Frequency).

The regression value of the surface (r^2) of the calibration curve is 0.9946, and the standard deviation is 0.0175 for the best calibration curve. The output voltage increases with increasing GVF. The superior performance is obtained from L12-R10 combination, and the 100 kHz is the optimum frequency of electrical impedance probe for the gas volume fraction measurement.

Figure 6.8 shows the calculated GVF as a function of GVF, and Figure 6.9 shows the differences of the calculated GVF and measured GVF as a function of GVF.

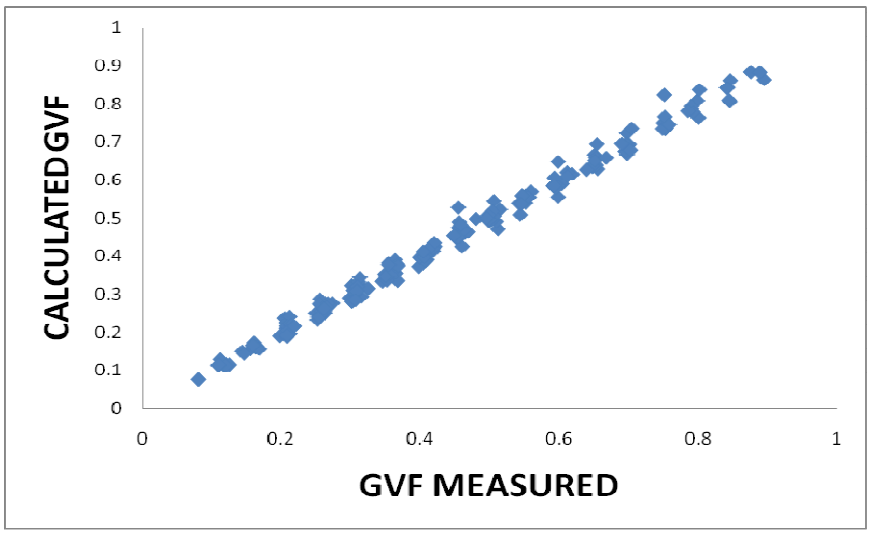

Figure 6.8 The Calculated GVF As A Function Of GVF.

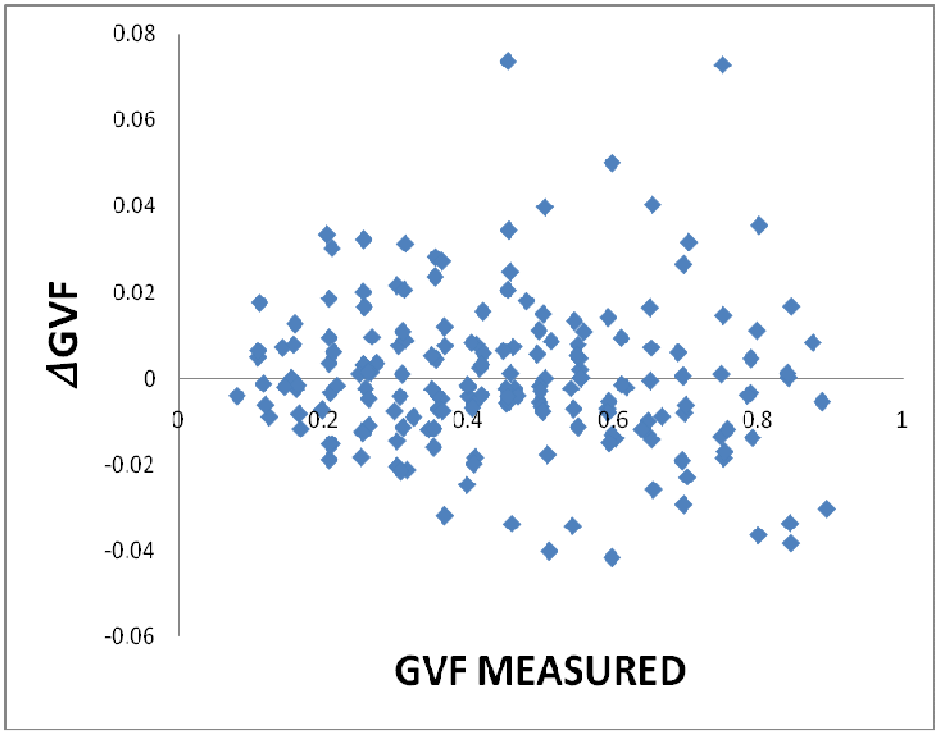

Figure 6.9 The Error Of GVF And The Measured GVF (As A Function Of GVF).

The figure also presents that the standard deviation of the Figure 6.7 correspond with Figure 6.9, and thus the relation from Figure 6.7 is proper to use. The calculated GVF shows linearity with measured GVF.

One hundred kHz is the best frequency for all positions. The other frequencies also show good response to measured GVF; however, the 13 kHz failed to reach the same performance for this purpose. Even though the 13 kHz is the worst frequency, the regression value of calibration curves of 13 kHz is higher than 0. 89. When the frequency increases after 100 kHz, the accuracy of the impedance sensor slightly

decreases for all positions. The table shows curve fitting results. The regression values in the calibration curves show that the effectives of the frequency changes are very low after 13 kHz for all positions. However, it is expected that 13 Hz should be the best frequency to measure air –oil mixture because of the capacitance ratio between air and oil less than capacitance ratio of water and air.

The following equation is used to calculate the GVF;

$$GVF = a + \frac{b}{T} + c\,LN(V) + \frac{d}{T^2} + e\,LN(V)^2 + f\,\frac{LN(V)}{T} + \frac{g}{T^3} + h\,LN(V)^3 + i\,\frac{LN(V)^2}{T} + j\frac{dLN(V)}{T^2}$$

When T is the temperature, V is the output voltage of the electrical impedance probe, and a= -3.312, b=-455.677, c=-9.741, d=149867.263, e=-1.255, f=1319.438, g=-6.752e+06, h= 0.042, i= 102.98 and j=-40564.818.

Table 6.1 shows the equations, the regression values and the standard deviations from calibration curves are given to determine GVF.

Table 6.1 The equations, the regression values and the standard deviations (from calibration curves are given to determine GVF).

Position	Freq kHz	Curve fitting equation Z= GVF X=Temperature Y= Voltage	R^2	StdV
L10 R10	13	z=a+b/x+cy+d/x^2+ey^2+fy/x+g/x^3+hy^3+iy^2/x +jy/x^2	0.94	0.054
	57	z=a+b/x+clny+d/x^2+e(lny)^2+f(lny)/x+g/x^3+h(ln y)^3+i(lny)^2/x+j(lny)/x^2	0.99	0.021
	100	z=a+b/x+clny+d/x^2+e(lny)^2+f(lny)/x+g/x^3+h(ln y)^3+i(lny)^2/x+j(lny)/x^2	0.99	0.021
	143	z=a+b/x+clny+d/x^2+e(lny)^2+f(lny)/x+g/x^3+h(ln y)^3+i(lny)^2/x+j(lny)/x^2	0.99	0.021
	187	z=a+b/x+clny+d/x^2+e(lny)^2+f(lny)/x+g/x^3+h(ln y)^3+i(lny)^2/x+j(lny)/x^2	0.99	0.991
	230	z=a+b/x+clny+d/x^2+e(lny)^2+f(lny)/x+g/x^3+h(ln y)^3+i(lny)^2/x+j(lny)/x^2	0.99	0.021
	273	z=a+b/x+clny+d/x^2+e(lny)^2+f(lny)/x+g/x^3+h(ln y)^3+i(lny)^2/x+j(lny)/x^2	0.99	0.021
	317	z=a+b/x+clny+d/x^2+e(lny)^2+f(lny)/x+g/x^3+h(ln y)^3+i(lny)^2/x+j(lny)/x^2	0.99	0.021
	360	z=a+bx+clny+dx^2+e(lny)^2+fxlny+gx^3+h(lny)^3 +ix(lny)^2+jx^2lny	0.99	0.022

Table 6.1 Continued

Position	Freq kHz	Curve fitting equation Z= GVF X=Temperature Y= Voltage	R^2	StdV
	403	z=a+b/x+clny+d/x^2+e(lny)^2+f(lny)/x+g/x^3+h(lny)^3+i(lny)^2/x+j(lny)/x^2	0.99	0.022
L10 R11	13	z=a+bx+cy+dx^2+ey^2+fxy	0.90	0.074
	57	z=a+b/x+clny+d/x^2+e(lny)^2+f(lny)/x+g/x^3+h(lny)^3+i(lny)^2/x+j(lny)/x^2	0.99	0.021
	100	z=a+b/x+clny+d/x^2+e(lny)^2+f(lny)/x+g/x^3+h(lny)^3+i(lny)^2/x+j(lny)/x^2	0.99	0.020
	143	z=a+b/x+clny+d/x^2+e(lny)^2+f(lny)/x+g/x^3+h(lny)^3+i(lny)^2/x+j(lny)/x^2	0.99	0.020
	187	z=a+b/x+clny+d/x^2+e(lny)^2+f(lny)/x+g/x^3+h(lny)^3+i(lny)^2/x+j(lny)/x^2	0.99	0.020
	230	z=a+b/x+clny+d/x^2+e(lny)^2+f(lny)/x+g/x^3+h(lny)^3+i(lny)^2/x+j(lny)/x^2	0.99	0.020
	273	z=a+b/x+clny+d/x^2+e(lny)^2+f(lny)/x+g/x^3+h(lny)^3+i(lny)^2/x+j(lny)/x^2	0.99	0.020
	317	z=a+b/x+clny+d/x^2+e(lny)^2+f(lny)/x+g/x^3+h(lny)^3+i(lny)^2/x+j(lny)/x^2	0.99	0.021
	360	z=a+b/x+clny+d/x^2+e(lny)^2+f(lny)/x+g/x^3+h(lny)^3+i(lny)^2/x+j(lny)/x^2	0.99	0.021

Table 6.1 Continued

Position	Freq kHz	Curve fitting equation Z= GVF X=Temperature Y= Voltage	R^2	StdV
L10 R12	13	z=a+bx+cx^2+dx^3+ex^4+fx^5+glny+h(lny)^2+i(lny)^3+j(lny)^4	0.95	0.052
	57	z=a+b/x+clny+d/x^2+e(lny)^2+f(lny)/x+g/x^3+h(lny)^3+i(lny)^2/x+j(lny)/x^2	0.99	0.019
	100	z=a+b/x+clny+d/x^2+e(lny)^2+f(lny)/x+g/x^3+h(lny)^3+i(lny)^2/x+j(lny)/x^2	0.93	0.019
	143	z=a+b/x+clny+d/x^2+e(lny)^2+f(lny)/x+g/x^3+h(lny)^3+i(lny)^2/x+j(lny)/x^2	0.99	0.019
	187	z=a+b/x+clny+d/x^2+e(lny)^2+f(lny)/x+g/x^3+h(lny)^3+i(lny)^2/x+j(lny)/x^2	0.99	0.019
	230	z=a+b/x+clny+d/x^2+e(lny)^2+f(lny)/x+g/x^3+h(lny)^3+i(lny)^2/x+j(lny)/x^2	0.99	0.019
	273	z=a+b/x+clny+d/x^2+e(lny)^2+f(lny)/x+g/x^3+h(lny)^3+i(lny)^2/x+j(lny)/x^2	0.99	0.020
	317	z=a+b/x+clny+d/x^2+e(lny)^2+f(lny)/x+g/x^3+h(lny)^3+i(lny)^2/x+j(lny)/x^2	0.99	0.020
	360	z=a+b/x+clny+d/x^2+e(lny)^2+f(lny)/x+g/x^3+h(lny)^3+i(lny)^2/x+j(lny)/x^2	0.99	0.020

Table 6.1 Continued

Position	Freq kHz	Curve fitting equation Z= GVF X=Temperature Y= Voltage	R^2	StdV
L11 R10	13	z=a+b/x+c/y+d/x^2+e/y^2+f/(xy)+g/x^3+h/y^3+i/(xy^2)+j/(x^2y)	0.97	0.034
	57	z=a+b/x+clny+d/x^2+e(lny)^2+f(lny)/x+g/x^3+h(lny)^3+i(lny)^2/x+j(lny)/x^2	0.99	0.019
	100	z=a+b/x+clny+d/x^2+e(lny)^2+f(lny)/x+g/x^3+h(lny)^3+i(lny)^2/x+j(lny)/x^2	0.99	0.019
	143	z=a+b/x+clny+d/x^2+e(lny)^2+f(lny)/x+g/x^3+h(lny)^3+i(lny)^2/x+j(lny)/x^2	0.99	0.019
	187	z=a+b/x+clny+d/x^2+e(lny)^2+f(lny)/x+g/x^3+h(lny)^3+i(lny)^2/x+j(lny)/x^2	0.99	0.019
	230	z=a+b/x+clny+d/x^2+e(lny)^2+f(lny)/x+g/x^3+h(lny)^3+i(lny)^2/x+j(lny)/x^2	0.99	0.019
	273	z=a+b/x+clny+d/x^2+e(lny)^2+f(lny)/x+g/x^3+h(lny)^3+i(lny)^2/x+j(lny)/x^2	0.99	0.019
	317	z=a+b/x+clny+d/x^2+e(lny)^2+f(lny)/x+g/x^3+h(lny)^3+i(lny)^2/x+j(lny)/x^2	0.99	0.019
	360	z=a+b/x+clny+d/x^2+e(lny)^2+f(lny)/x+g/x^3+h(lny)^3+i(lny)^2/x+j(lny)/x^2	0.99	0.019
	403	z=a+b/x+clny+d/x^2+e(lny)^2+f(lny)/x+g/x^3+h(lny)^3+i(lny)^2/x+j(lny)/x^2	0.99	0.019

Table 6.1 Continued

Position	Freq kHz	Curve fitting equation Z= GVF X=Temperature Y= Voltage	R^2	StdV
	100	z=a+b/x+clny+d/x^2+e(lny)^2+f(lny)/x+g/x^3+h(lny)^3+i(lny)^2/x+j(lny)/x^2	0.99	0.021
	143	z=a+b/x+clny+d/x^2+e(lny)^2+f(lny)/x+g/x^3+h(lny)^3+i(lny)^2/x+j(lny)/x^2	0.99	0.021
	187	z=a+b/x+clny+d/x^2+e(lny)^2+f(lny)/x+g/x^3+h(lny)^3+i(lny)^2/x+j(lny)/x^2	0.99	0.021
	230	z=a+b/x+clny+d/x^2+e(lny)^2+f(lny)/x+g/x^3+h(lny)^3+i(lny)^2/x+j(lny)/x^2	0.99	0.021
	273	z=a+b/x+clny+d/x^2+e(lny)^2+f(lny)/x+g/x^3+h(lny)^3+i(lny)^2/x+j(lny)/x^2	0.99	.0220
	317	z=a+b/x+clny+d/x^2+e(lny)^2+f(lny)/x+g/x^3+h(lny)^3+i(lny)^2/x+j(lny)/x^2	0.99	0.022
	360	z=a+b/x+clny+d/x^2+e(lny)^2+f(lny)/x+g/x^3+h(lny)^3+i(lny)^2/x+j(lny)/x^2	0.99	0.022
	403	z=a+b/x+clny+d/x^2+e(lny)^2+f(lny)/x+g/x^3+h(lny)^3+i(lny)^2/x+j(lny)/x^2	0.99	0.022
	13	z=a+b/x+clny+d/x^2+e(lny)^2+f(lny)/x+g/x^3+h(lny)^3+i(lny)^2/x+j(lny)/x^2	0.98	0.030

Table 6.1 Continued

Position	Freq kHz	Curve fitting equation Z= GVF X=Temperature Y= Voltage	R^2	StdV
L11 R12	100	z=a+b/x+clny+d/x^2+e(lny)^2+f(lny)/x+g/x^3+h(lny)^3+i(lny)^2/x+j(lny)/x^2	0.99	0.019
	143	z=a+b/x+clny+d/x^2+e(lny)^2+f(lny)/x+g/x^3+h(lny)^3+i(lny)^2/x+j(lny)/x^2	0.99	0.019
	187	z=a+b/x+clny+d/x^2+e(lny)^2+f(lny)/x+g/x^3+h(lny)^3+i(lny)^2/x+j(lny)/x^2	0.99	0.019
	230	z=a+b/x+clny+d/x^2+e(lny)^2+f(lny)/x+g/x^3+h(lny)^3+i(lny)^2/x+j(lny)/x^2	0.99	0.019
	273	z=a+b/x+clny+d/x^2+e(lny)^2+f(lny)/x+g/x^3+h(lny)^3+i(lny)^2/x+j(lny)/x^2	0.99	0.019
	317	z=a+b/x+clny+d/x^2+e(lny)^2+f(lny)/x+g/x^3+h(lny)^3+i(lny)^2/x+j(lny)/x^2	0.99	0.020
	360	z=a+b/x+clny+d/x^2+e(lny)^2+f(lny)/x+g/x^3+h(lny)^3+i(lny)^2/x+j(lny)/x^2	0.99	0.020
	403	z=a+b/x+clny+d/x^2+e(lny)^2+f(lny)/x+g/x^3+h(lny)^3+i(lny)^2/x+j(lny)/x^2	0.99	0.020
	57	z=a+b/x+clny+d/x^2+e(lny)^2+f(lny)/x+g/x^3+h(lny)^3+i(lny)^2/x+j(lny)/x^2	0.99	0.018

Table 6.1 Continued

Position	Freq kHz	Curve fitting equation Z= GVF X=Temperature Y= Voltage	R^2	StdV
	100	z=a+b/x+clny+d/x^2+e(lny)^2+f(lny)/x+g/x^3+h(lny)^3+i(lny)^2/x+j(lny)/x^2	0.99	0.017
	143	z=a+b/x+clny+d/x^2+e(lny)^2+f(lny)/x+g/x^3+h(lny)^3+i(lny)^2/x+j(lny)/x^2	0.99	0.017
	187	z=a+b/x+clny+d/x^2+e(lny)^2+f(lny)/x+g/x^3+h(lny)^3+i(lny)^2/x+j(lny)/x^2	0.99	0.017
	230	z=a+b/x+clny+d/x^2+e(lny)^2+f(lny)/x+g/x^3+h(lny)^3+i(lny)^2/x+j(lny)/x^2	0.99	0.017
	273	z=a+b/x+clny+d/x^2+e(lny)^2+f(lny)/x+g/x^3+h(lny)^3+i(lny)^2/x+j(lny)/x^2	0.99	0.017
	317	z=a+b/x+clny+d/x^2+e(lny)^2+f(lny)/x+g/x^3+h(lny)^3+i(lny)^2/x+j(lny)/x^2	0.99	0.017
	360	z=a+b/x+clny+d/x^2+e(lny)^2+f(lny)/x+g/x^3+h(lny)^3+i(lny)^2/x+j(lny)/x^2	0.99	0.017
	403	z=a+b/x+clny+d/x^2+e(lny)^2+f(lny)/x+g/x^3+h(lny)^3+i(lny)^2/x+j(lny)/x^2	0.99	0.017
	13	z=a+b/x+c/y+d/x^2+e/y^2+f/(xy)+g/x^3+h/y^3+i/(xy^2)+j/(x^2y)	0.94	0.054
	57	z=a+b/x+clny+d/x^2+e(lny)^2+f(lny)/x+g/x^3+h(lny)^3+i(lny)^2/x+j(lny)/x^2	0.99	0.019

Table 6.1 Continued

Position	Freq kHz	Curve fitting equation Z= GVF X=Temperature Y= Voltage	R^2	StdV
L12 R11	100	z=a+b/x+clny+d/x^2+e(lny)^2+f(lny)/x+g/x^3+h(lny)^3+i(lny)^2/x+j(lny)/x^2	0.99	0.017
	143	z=a+b/x+clny+d/x^2+e(lny)^2+f(lny)/x+g/x^3+h(lny)^3+i(lny)^2/x+j(lny)/x^2	0.99	0.017
	187	z=a+b/x+clny+d/x^2+e(lny)^2+f(lny)/x+g/x^3+h(lny)^3+i(lny)^2/x+j(lny)/x^2	0.99	0.017
	230	z=a+b/x+clny+d/x^2+e(lny)^2+f(lny)/x+g/x^3+h(lny)^3+i(lny)^2/x+j(lny)/x^2	0.99	0.018
	273	z=a+b/x+clny+d/x^2+e(lny)^2+f(lny)/x+g/x^3+h(lny)^3+i(lny)^2/x+j(lny)/x^2	0.99	0.018
	317	z=a+b/x+clny+d/x^2+e(lny)^2+f(lny)/x+g/x^3+h(lny)^3+i(lny)^2/x+j(lny)/x^2	0.99	0.018
	360	z=a+b/x+clny+d/x^2+e(lny)^2+f(lny)/x+g/x^3+h(lny)^3+i(lny)^2/x+j(lny)/x^2	0.99	0.018
	403	z=a+b/x+clny+d/x^2+e(lny)^2+f(lny)/x+g/x^3+h(lny)^3+i(lny)^2/x+j(lny)/x^2	0.99	0.018

Table 6.1 Continued

Position	Freq kHz	Curve fitting equation Z= GVF X=Temperature Y= Voltage	R^2	StdV
L12 R12	57	z=a+b/x+clny+d/x^2+e(lny)^2+f(lny)/x+g/x^3+h(lny)^3+i(lny)^2/x+j(lny)/x^2	0.99	0.020
	100	z=a+b/x+clny+d/x^2+e(lny)^2+f(lny)/x+g/x^3+h(lny)^3+i(lny)^2/x+j(lny)/x^2	0.99	0.019
	143	z=a+b/x+clny+d/x^2+e(lny)^2+f(lny)/x+g/x^3+h(lny)^3+i(lny)^2/x+j(lny)/x^2	0.99	0.019
	187	z=a+b/x+clny+d/x^2+e(lny)^2+f(lny)/x+g/x^3+h(lny)^3+i(lny)^2/x+j(lny)/x^2	0.99	0.019
	230	z=a+b/x+clny+d/x^2+e(lny)^2+f(lny)/x+g/x^3+h(lny)^3+i(lny)^2/x+j(lny)/x^2	0.99	0.019
	317	z=a+b/x+clny+d/x^2+e(lny)^2+f(lny)/x+g/x^3+h(lny)^3+i(lny)^2/x+j(lny)/x^2	0.99	0.019
	360	z=a+b/x+clny+d/x^2+e(lny)^2+f(lny)/x+g/x^3+h(lny)^3+i(lny)^2/x+j(lny)/x^2	0.99	0.016

6.3. The Slotted Orifice Plate

The differential pressure, the density of air, the effective pipe diameter and the given mass flow rate of mixture were used to calculate KY. Quality was calculated by using the GVF meter. The KY, the quality and the gauge pressure were used for curve fitting and gathering proper correlation {KY (Q, P)}. The defined KY from correlation was used to calculate the mass flow rate of mixture.

GVF value was only provided from the electrical impedance probe because the GVF from the swirl-meter is not adequate to due to limited range of GVF. Figure 6.10 shows the calibration curve for the slotted plate. The regression value of the surface (r^2) of the calibration curve for KY is 0.9567.

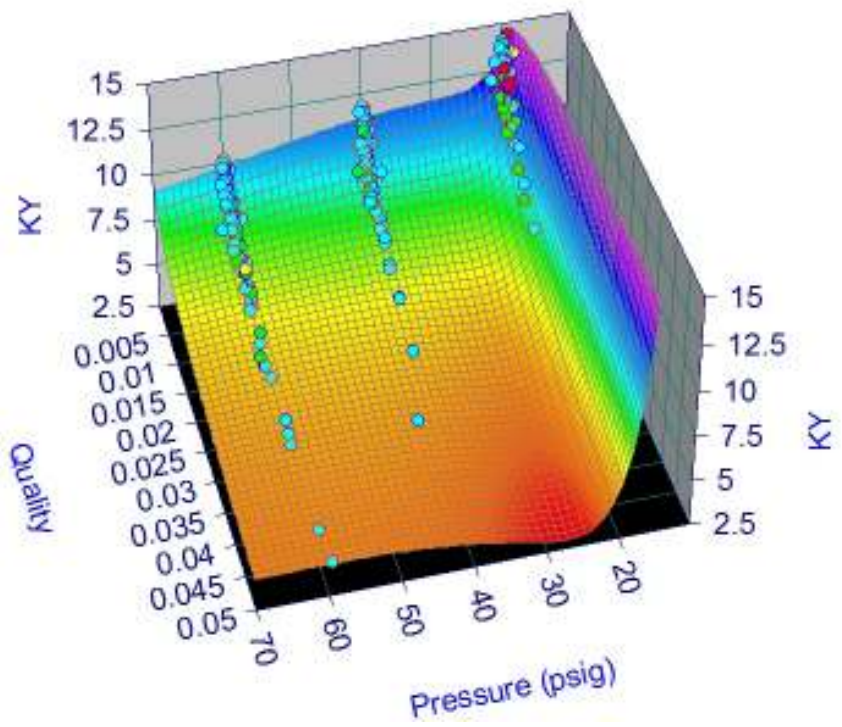

Figure 6.10 The Calibration Curve.

The Figure 6.11 displays the differences of the calculated total and measured total mass as a function of total mass. The figure also presents that the standard deviation of the Figure 6.10 correspond with Figure 6.11, and thus the relation from Figure 6.10 is proper to use.

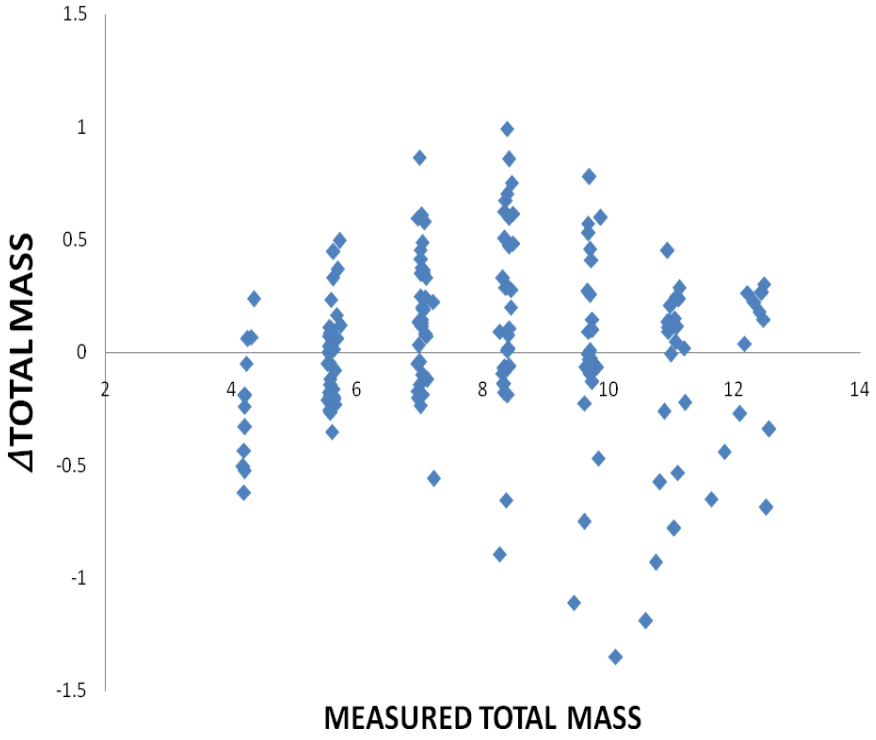

Figure 6.11 The Error Of Total And The Measured Total Mass As A Function Of Total Mass.

This study shows that the slotted plate in series with the impedance electrical probe can be used to determine the flow rate of the two-phase flow components. The standard deviation of the total mass is 0.38 lbm/ sec is presented over the range of 4 to 13 lbm/ sec, and the standard deviation of the GVF is 0.017 over the range of 10 to 95 %.

7. CONCLUSION

The objective of this study was to evaluate two different non-nuclear multiphase flow meters with a wide GVF range (covers gas to pure water), and to define the optimum operating conditions of these devices.

The first investigation looked at the accuracy of GVF measurement at varying GVFs, water flow rates, and pressures. The second investigation defined the operating condition and the operating frequency of the flow meters at varying positions and frequencies, GVFs, water flow rates, and pressures. The third investigation determined the accuracy of the mass flow rates of the mixture at varying GVFs, water flow rates, and pressures.

7.1. The Accuracy Performance Of GVF Metering

Two different devices were used to provide GVF measurement in different experimental setups. The slotted plate was used because of its independence of upstream flow conditions, good response in two-phase flow, and ability to produce well homogenized downstream flow. Thus, the well homogenized flow increases GVF measurement accuracy.

The swirl-meter frequency output is repeatable for higher than 60%GVF, and the frequency variation is associated with GVF and test section pressure. Where the GVF is less than 60%, the accuracy of the measurement is due to the fluctuation of the frequency. Although the inaccuracy of the initial measurement was high, and the

standard deviation was 0.08, the error showed linear response to the GVF. Another relation established between the errors, the GVF and the density of the mixture reduced the inaccuracy. The new standard deviation of GVF measurement was 0.002. This shows that the swirl-meter is a promising device to measure GVF in industrial applications.

The electrical impedance probes provide accurate measurement within the 10% to 100 % GVF range. The error of the GVF measurement is 0.017. The sensitivity of the device is not enough to obtain accurate results for less than 10% GVF, and thus the output voltage is very close to 0. The slotted plate provides adequate homogenized downstream flow for probes. The electrical impedance probes can safely be used for GVF measurement with high accuracy. Because of the wide operating range, they are suitable to use in industrial applications.

7.2. The Operating Condition Of The GVF Metering

The swirl-meter frequency output is repeatable for higher than 60%GVF, and after iteration, high accurate measurement can be provided. Even though the swirl-meter usually used to measure wet gas (is defined as a two-phase within range of 90 to 99% GVF), the operation range of GVF expanded to a total range of 60% to 100% due to well homogenized downstream flow of the slotted plate. It was also found that the test section pressure and density of the mixture are important factors for GVF measurement in the swirl-meter. The measurement is independent of temperature and water/ air flow rate.

The measurement with the electrical impedance probe is independent from the test section pressure and air /water flow rate. However, the measurement is dependent on the temperature. Although there is not significant accuracy differences in measurement for higher than 13 kHz, the 100 kHz is the best frequency for all positions. The 13 kHz failed to attain the same performance for measurement.

The probes were placed 10, 11, and 12 inches away from the slotted plate. The best position was L12-R10 because the measurement signal covers the largest volume. This position shows the highest accuracy.

7.3. The Accuracy Performance Of The Mass Flow Rate Of Mixture

The measurement of the mass flow rate of the mixture was provided from KY, quality, and pressure calibration curve. The accuracy of GVF is very important factor for the mass flow rate measurement because the quality revived from GVF. The electrical impedance probes were decided to measure mass flow because of large GVF range and high accuracy. The measurement error is 0.38 over the range of 4 to 13 lbm/sec. This shows that the electrical impedance probe -the slotted plate combination provide non-nuclear, cheap and high accurate measurement for two-phase flow.

7.4. Recommendations For The Future Work

In order to reach high accurate flow meters, more research needs to be performed.

- More investigations are conducted to measure less than 60% GVF from the swirl meter.
- The performance of the close coupled slotted plate and the electrical impedance probe can be evaluated for different mixtures components.
- The performance of the close coupled slotted plate and the electrical impedance probe can be evaluated for different pipe diameter and flow ranges.
- The performance of the close coupled slotted plate and the electrical impedance probe can be evaluated for three-phase flow.
- In case of sensitivity loss due to different mixtures components, the half ring shaped electrodes can be used to provide high accuracy.
- The closer probes positions can be investigated to reduce the length of the flow meter.

REFERENCES

[1] Hua CQ, Geng YF. Wet gas meter based on slotted orifice and swirl-meter performance in series. Measurement 2013; 30: 138-143.

[2] Thorn R., Johansen G.A., Hammer E.A., Recent developments in three-phase flow measurement. Measurement Science & Technology 1997; 8: 691–701.

[3] Morrison, G.L., Terracina, D., Brewer, C., Response of a slotted orifice flow meter to an air/ water mixture. Flow Measurement and Instrumentation 2001; 12:175-180.

[4] Morrison GL, Hall KR, Holste JC, Macek ML, Ihfe LM, DeOtte, Jr. RE, Terracina DP. Comparison of orifice and slotted plate flow-meters. Flow Measurement and Instrumentation 1994; 6:71-74.

[5] Geng, Y.F., Zheng, J.W., Shi, T.M., Study on the metering characteristics of a slotted orifice for wet gas flow. Flow Measurement and Instrumentation 2006; 17:123-128.

[6] Brewer C.V., Evaluation of the slotted orifice plate as a two phase flow meter, M.S. Thesis, Texas A&M University, College Station, TX, 1999

[7] Hall, K.R, Morrison, G.L., Slotted orifice flow meter, American Institute of Chemical Engineers Instrumentation Meeting 2000.

[8] Macek, M.L., A slotted orifice plate used as a flow measurement device, M. S. Thesis, Texas A&M University, College Station, TX, 1993.

[9] Ihfe L.M., Development of the slotted orifice flow conditioner, M.S. Thesis, Texas A&M University, College Station, TX, 1994

[10] Terracina D.P., The experimental and numerical development of the slotted plate, and its design parameter, M.S. Thesis, Texas A&M University, College Station, TX, 1996

[11] Flores, A.E., Evaluation of a slotted orifice plate flow meter using horizontal two phase flow, M.S. Thesis, Texas A&M University, College Station, TX, 2000

[12] Sparks S., The slotted plate has superior homogenizer performance than the standard orifice plate and V-cone, M.S. Thesis, Texas A&M University, College Station, TX, 2004

[13] Cascetta F., Scalabrini G., Field test of a swirl-meter for gas flow measurement, Flow Measurement and Instrumentation 1999; 10 (3):183–188.

[14] Goujon S. , Durand S., Technical note Linearity of the vortex meter as a function of fluid viscosity, Flow Measurement and Instrumentation 1995; 6 (3): 235-238.

[15] Sun Z. , Sang W., Zhang H., Measurement of pressure fluctuation in gas-liquid two phase vortex street, Journal of Physics 2009;147 012019

[16] Hua C.Q., Geng Y.F., Investigation on the swirl-meter performance in low pressure wet gas flow, Measurement 2011; 44 (5): 881–887.

[17] Miller R.W., Flow measurement engineering handbook, 2nd edn. New York: McGraw–Hill, 1989.

[18] Sun Z., Zhang H., Measurement of the flow rate and volume void fraction of gas liquid bubble flow using a vortex flow meter, Chemical Engineering Communications 2010;197:145–157.

[19] Uga T., Determination of the bubble size distribution in a boiling water reactor, Nuclear Engineering and Design 1972; 22:252-261

[20] Andreussi P, Di Donfrancesco A, Messia M. An impedance method for the measurement of liquid hold-up in two phase flow. International Journal of Multiphase Flow 1988; 14:777–85.

[21] Fossa M., Design and performance of a conductance probe for measuring the liquid fraction in two-phase gas-liquid flows, Flow Measurement and Instrumentation 1998;9: 103–109

[22] Devia F., Fossa M., Design and optimization of impedance probes for void fraction measurements, Flow Measurement and Instrumentation 2003; 14: 139–149

[23] Munholand L., Soucy G., Comparison of four conductive needle probe designs for determination of bubble velocity and local gas holdup. Review of Scientific Instruments 2005; 76: 095101.

[24] Da Silva M. J., Schleicher E., Hampel U., A novel needle probe based on high-speed complex permittivity measurements for investigation of dynamic fluid flows. IEEE Transactions in Instrumentation and Measurement 2007; 56: 4.

APPENDIX A

THE CALIBRATION CURVES

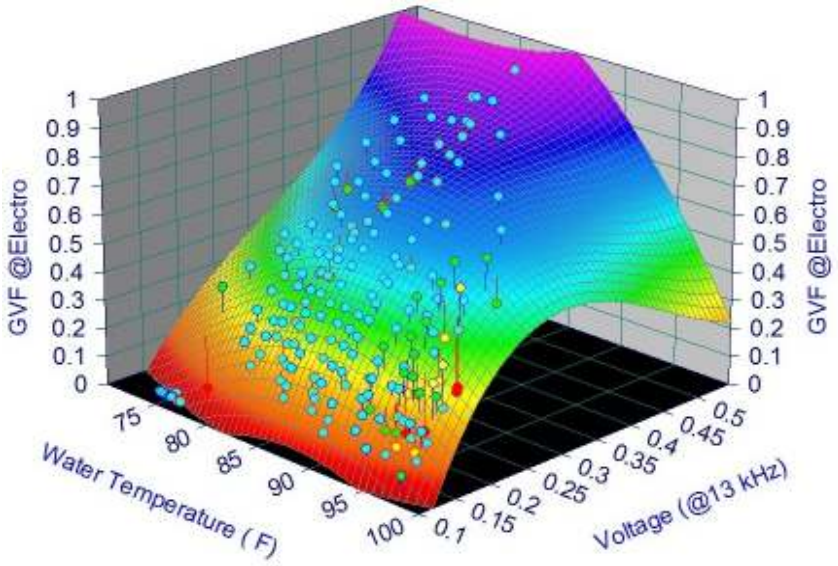

Figure7. 1 L10-R10 calibration curve at 13 KHz

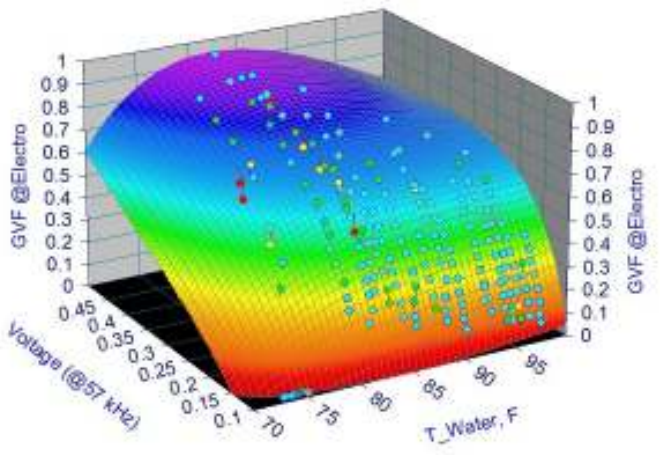

Figure7. 2 L10-R10 calibration curve at 57 KHz

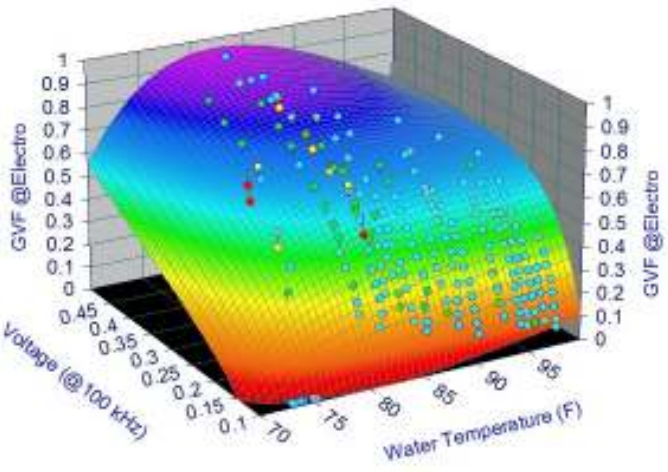

Figure7. 3 L10-R10 calibration curve at 100 KHz

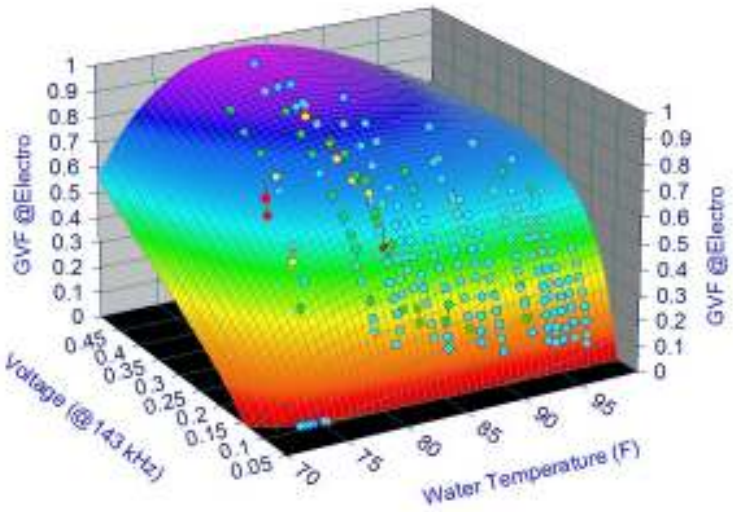

Figure7. 4 L10-R10 calibration curve at 143 KHz

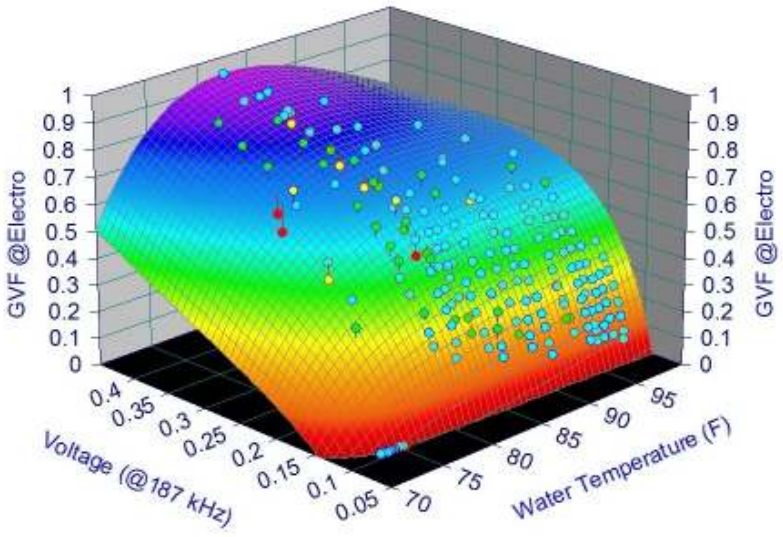

Figure7. 5 L10-R10 calibration curve at 187 KHz

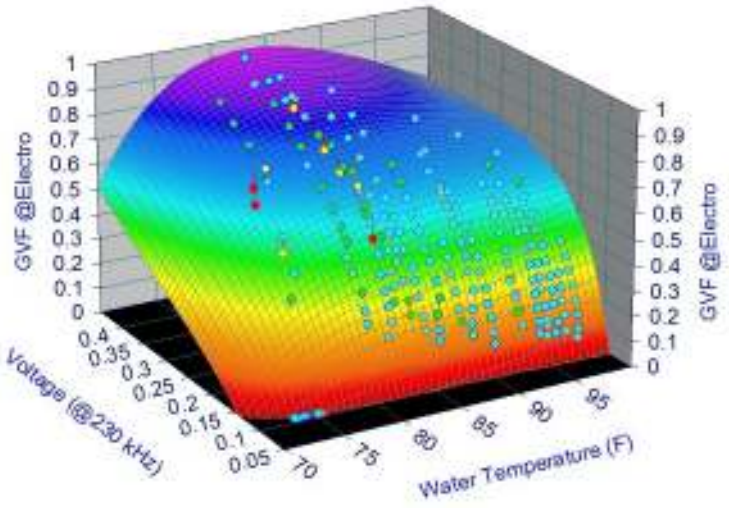

Figure7. 6 L10-R10 calibration curve at 230 KHz

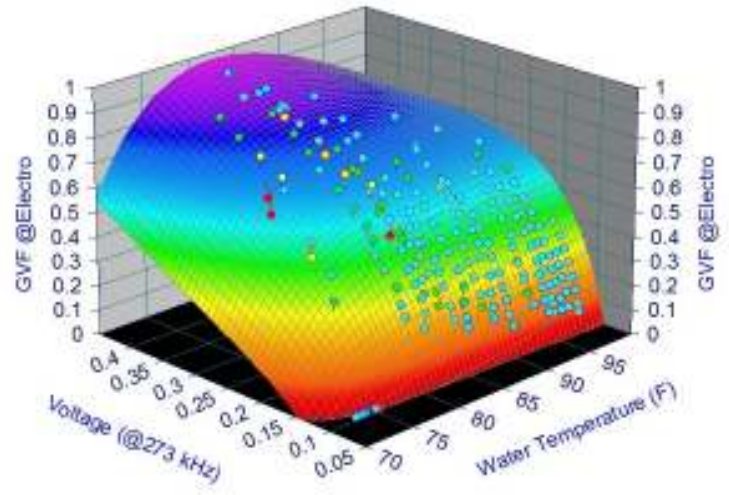

Figure7. 7 L10-R10 calibration curve at 273 KHz

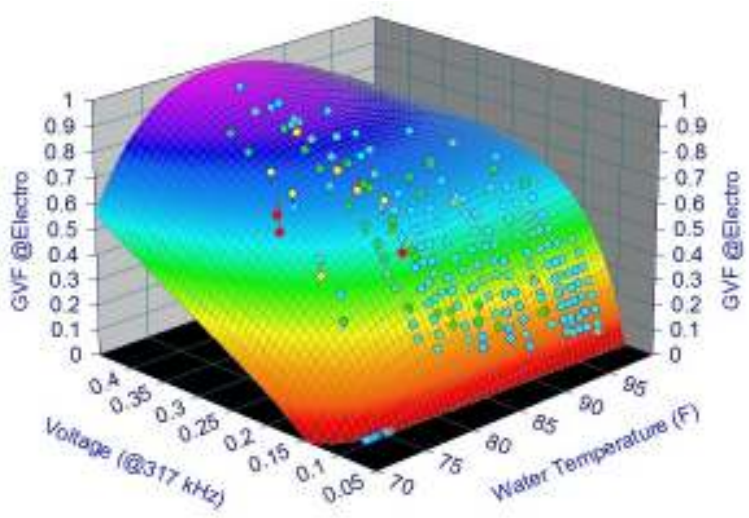

Figure7. 8 L10-R10 calibration curve at 317 KHz

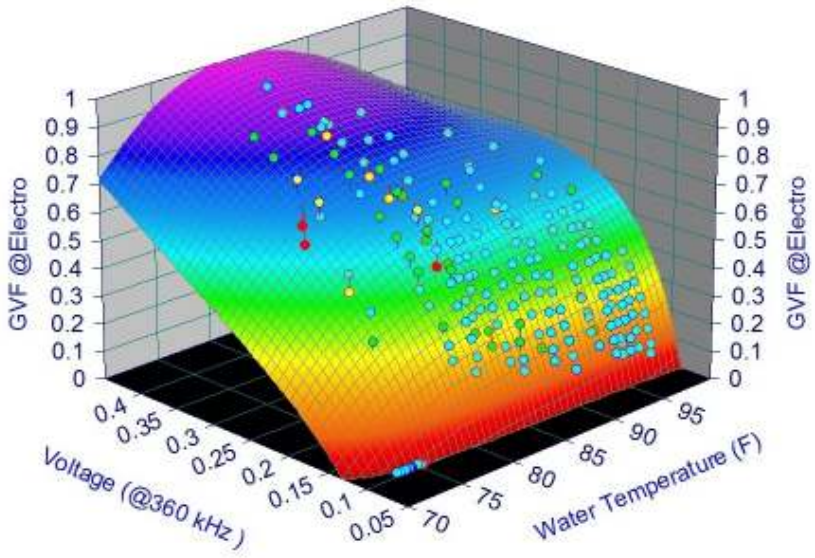

Figure7. 9 L10-R10 calibration curve at 360 KHz

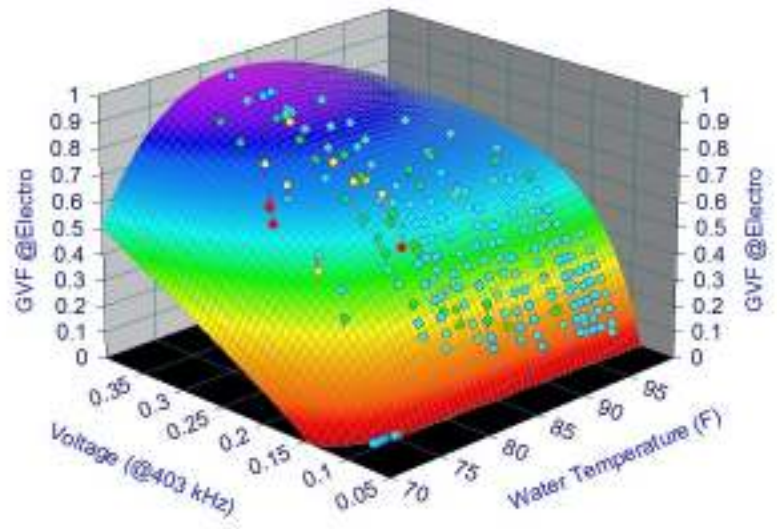

Figure7. 10 L10-R10 calibration curve at 403 KHz

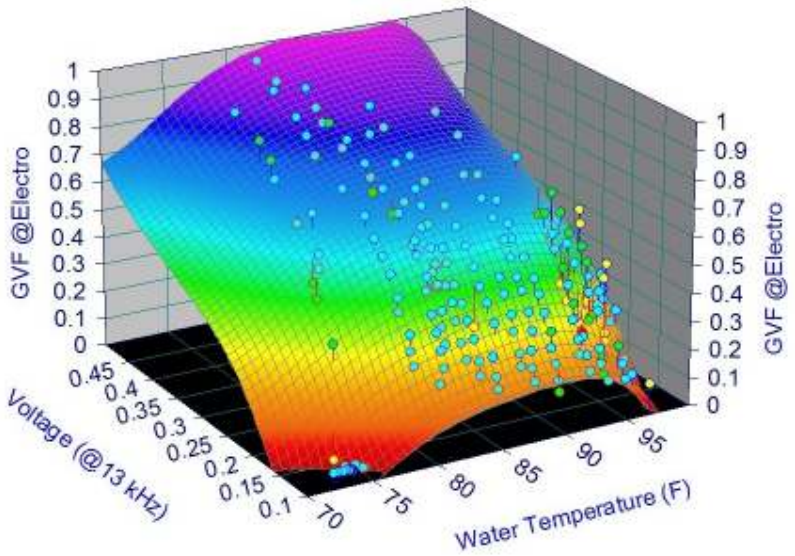

Figure7. 11 L10-R11 calibration curve at 13 KHz

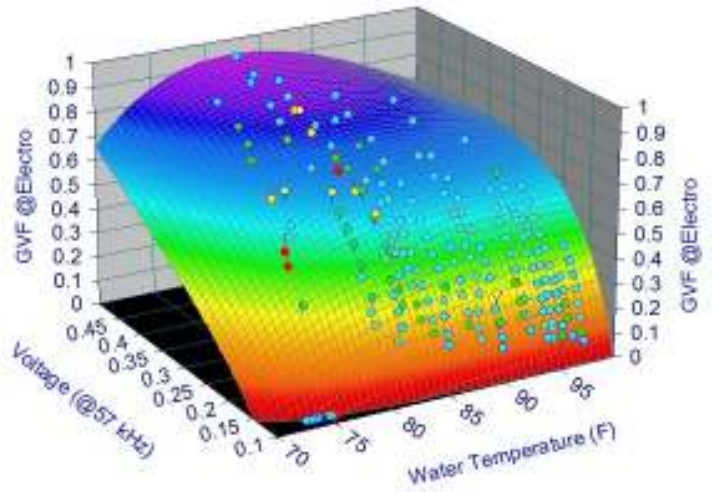

Figure7. 12 L10-R11 calibration curve at 57 KHz

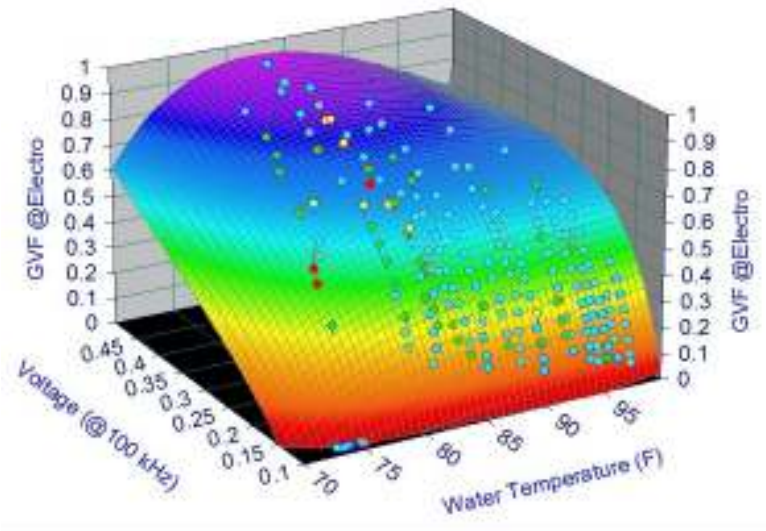

Figure7. 13 L10-R11 calibration curve at 100 KHz

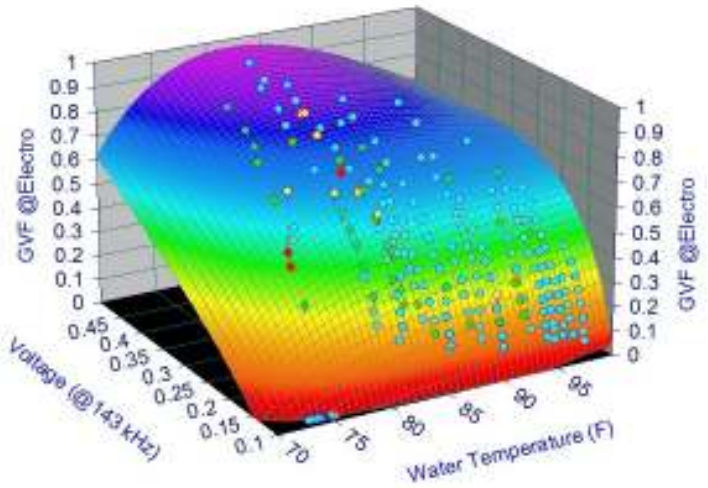

Figure7. 14 L10-R11 calibration curve at 143 KHz

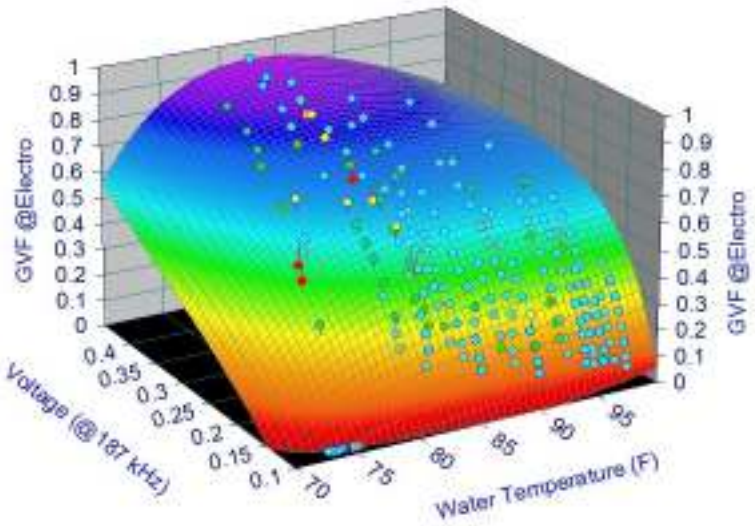

Figure7. 15 L10-R11 calibration curve at 187 KHz

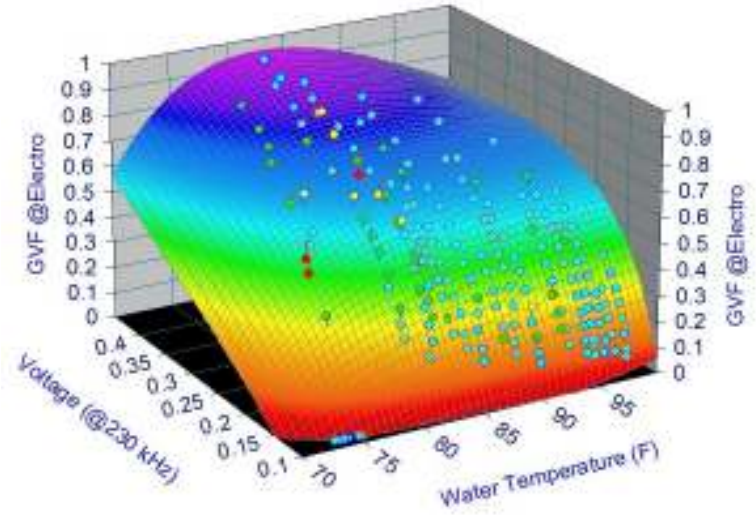

Figure7. 16 L10-R11 calibration curve at 213 KHz

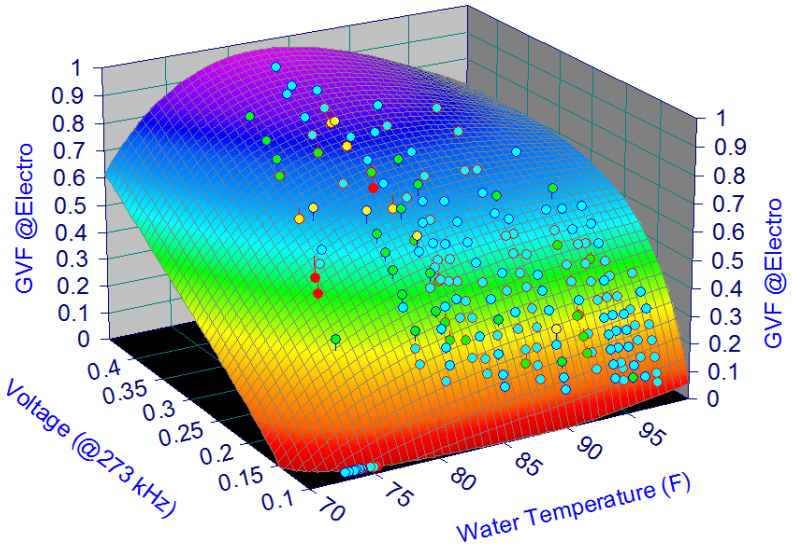

Figure7. 17 L10-R11 calibration curve at 273 KHz

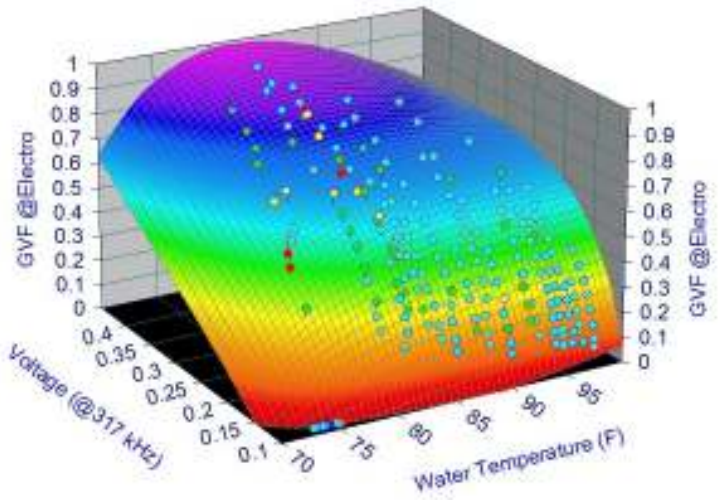

Figure7. 18 L10-R11 calibration curve at 317 KHz

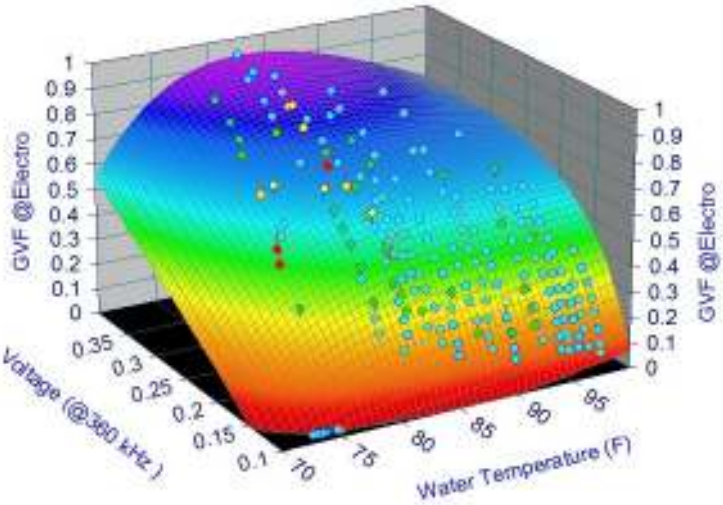

Figure7. 19 L10-R11 calibration curve at 360 KHz

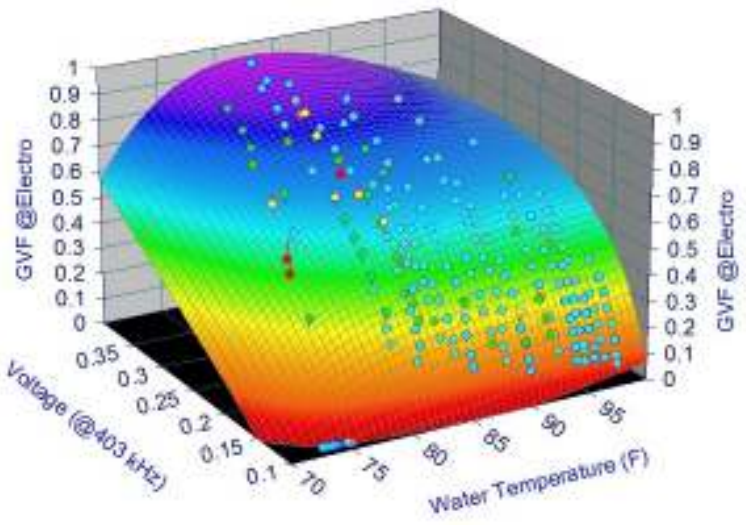

Figure7. 20 L10-R11 calibration curve at 403 KHz

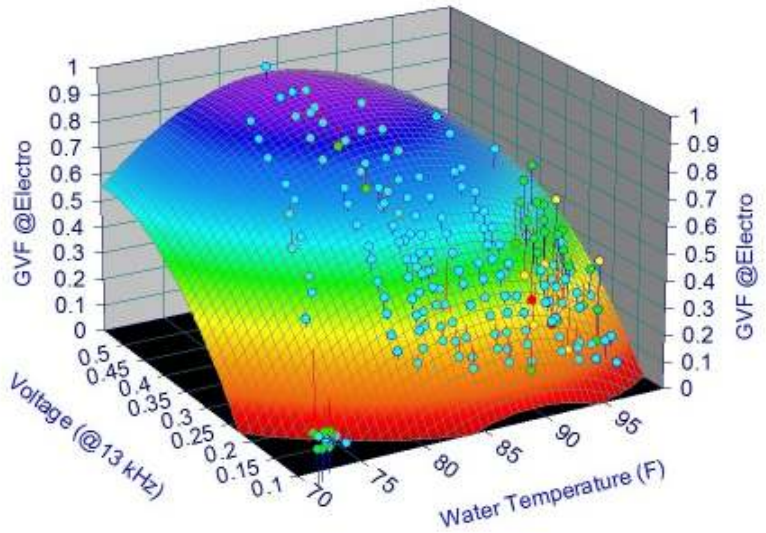

Figure7. 21 L10-R12 calibration curve at 13 KHz

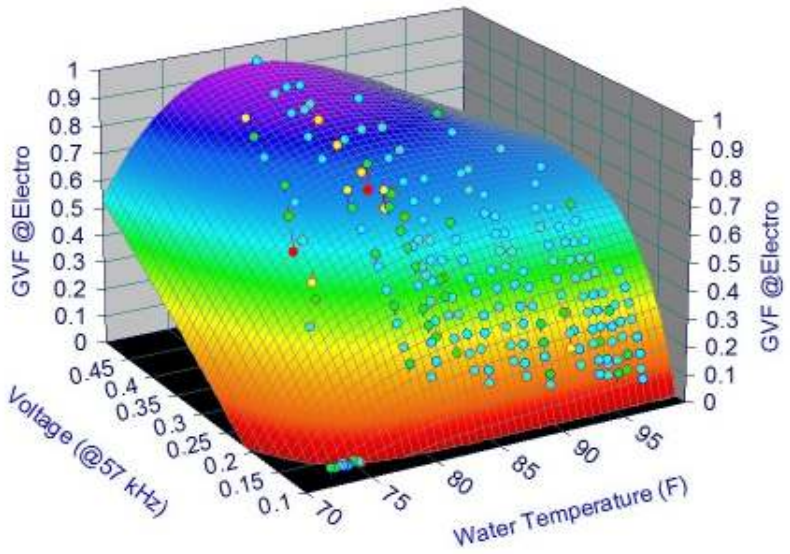

Figure7. 22 L10-R12 calibration curve at 57 KHz

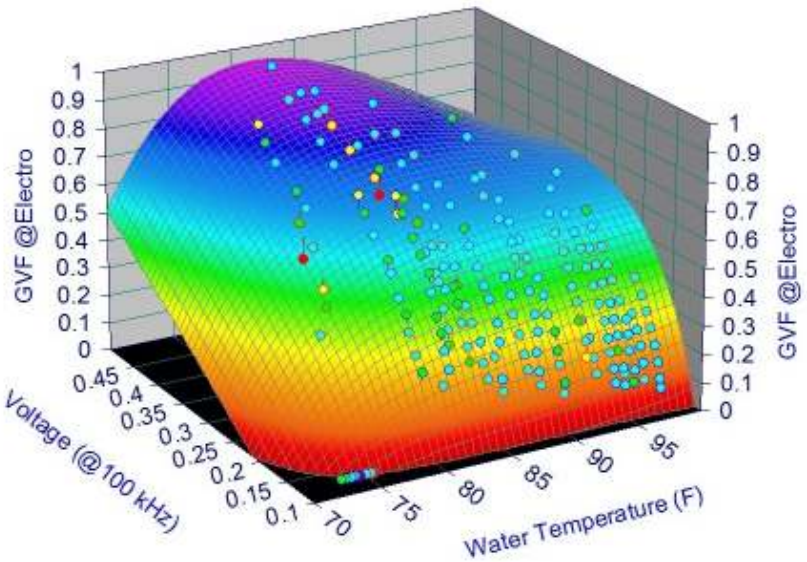

Figure7. 23 L10-R12 calibration curve at 100 KHz

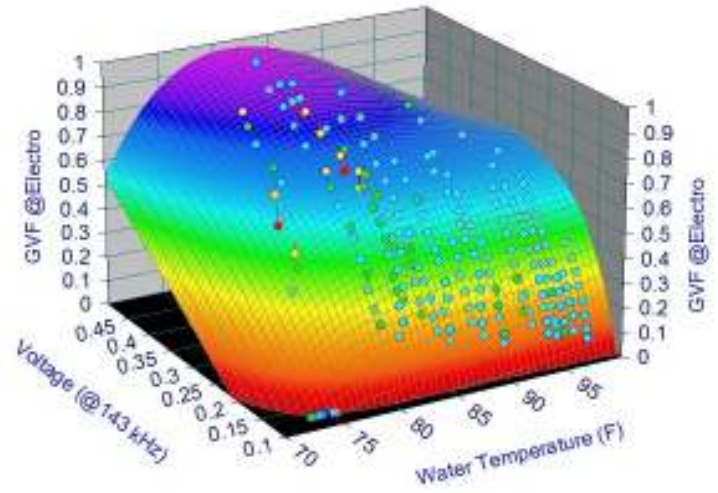

Figure7. 24 L10-R12 calibration curve at 143 KHz

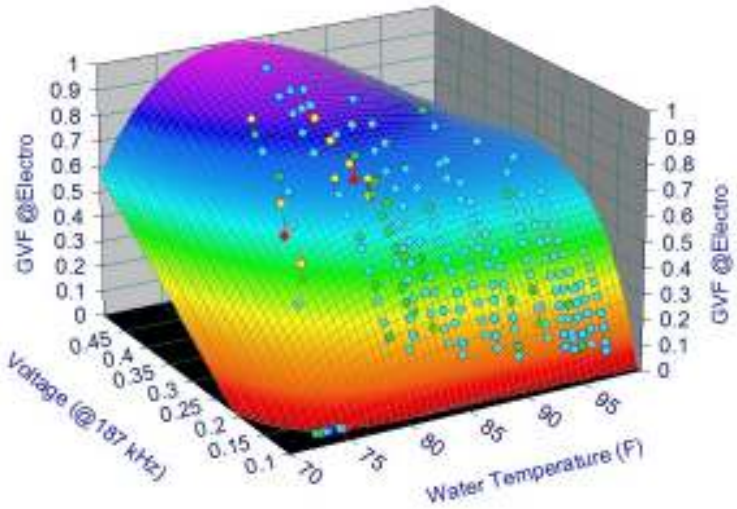

Figure7. 25 L10-R12 calibration curve at 187 KHz

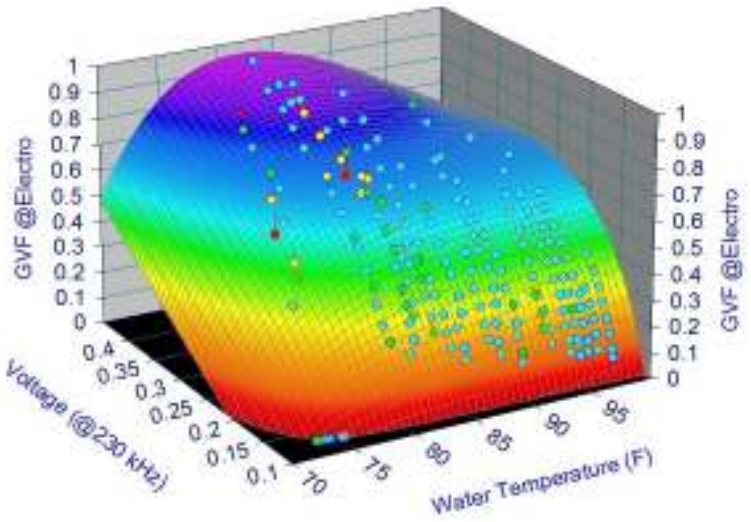

Figure7. 26 L10-R12 calibration curve at 230 KHz

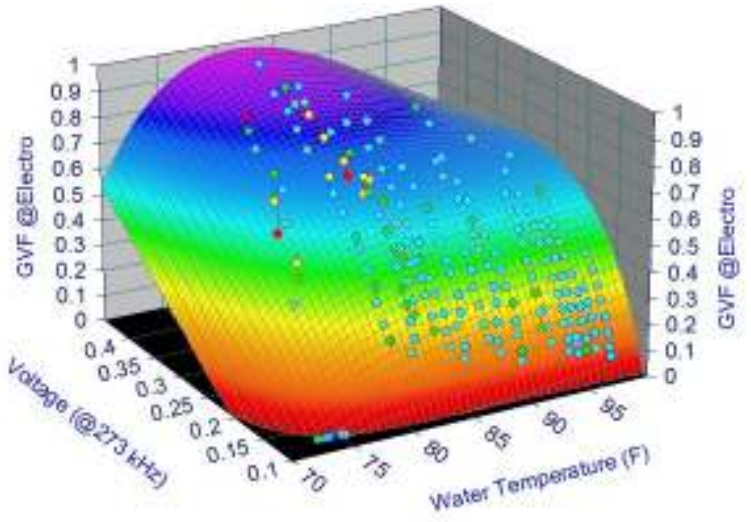

Figure7. 27 L10-R12 calibration curve at 273 KHz

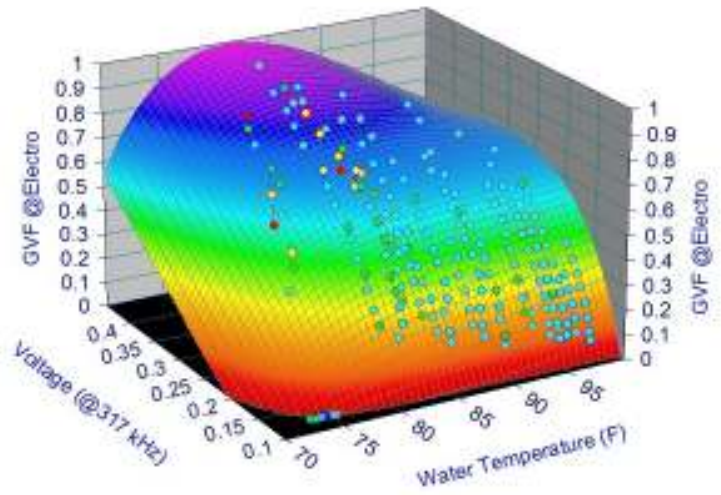

Figure7. 28 L10-R12 calibration curve at 317 KHz

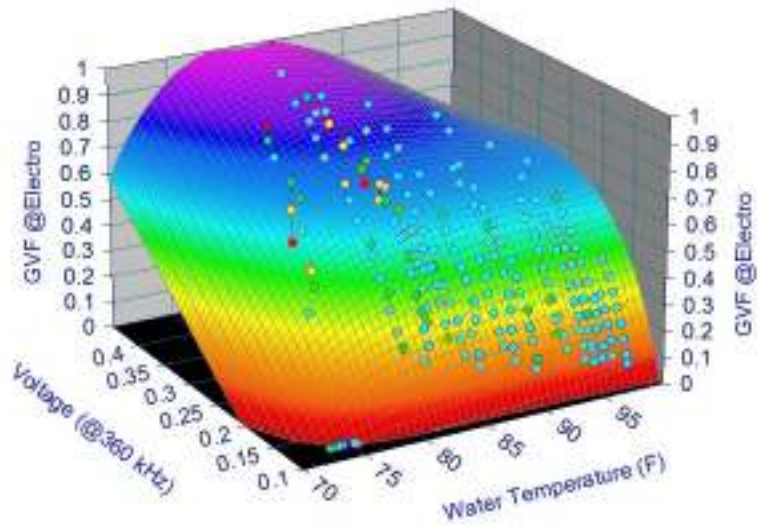

Figure7. 29 L10-R12 calibration curve at 360 KHz

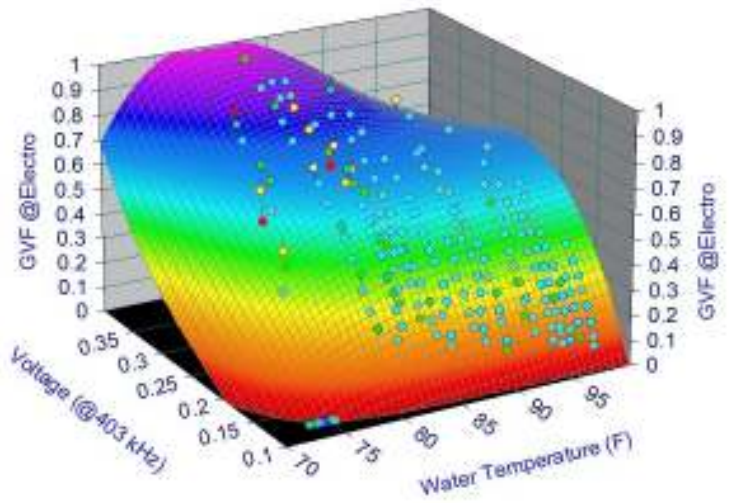

Figure7. 30 L10-R12 calibration curve at 403 KHz

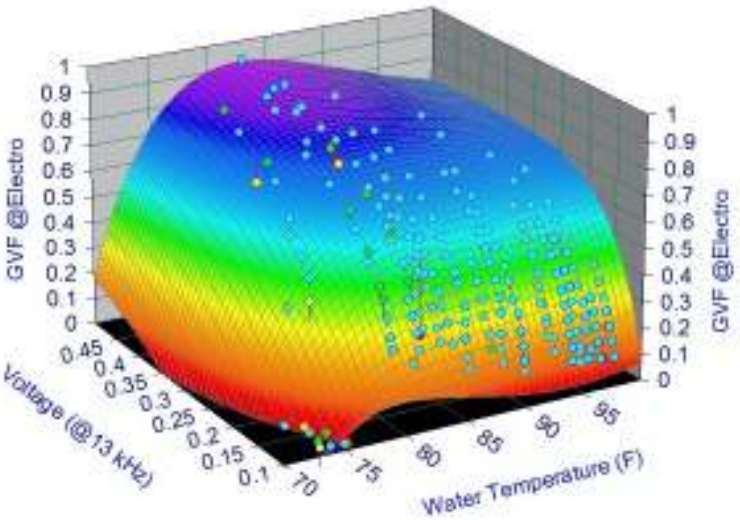

Figure7. 31 L11-R10 calibration curve at 13 KHz

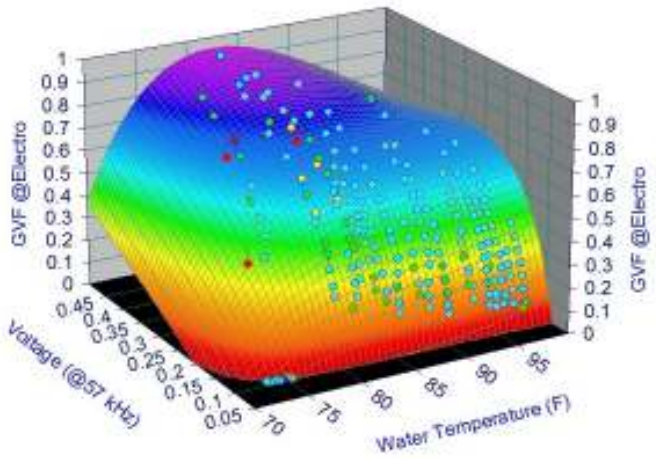

Figure7. 32 L11-R10 calibration curve at 57 KHz

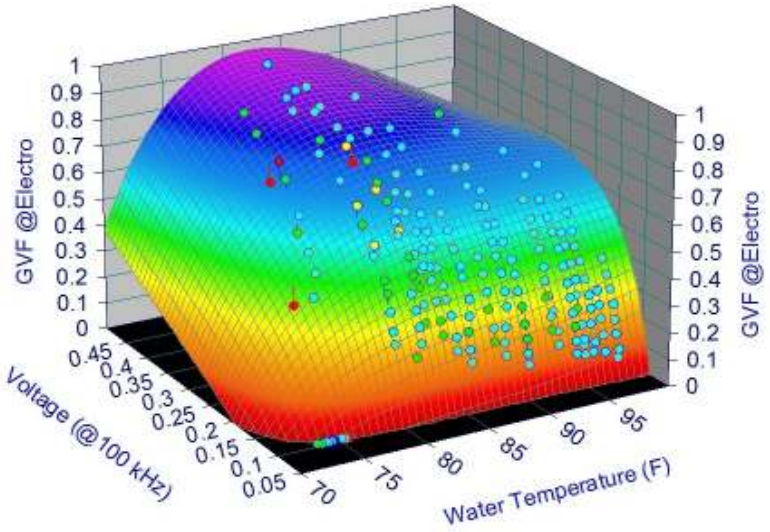

Figure7. 33 L11-R10 calibration curve at 100 KHz

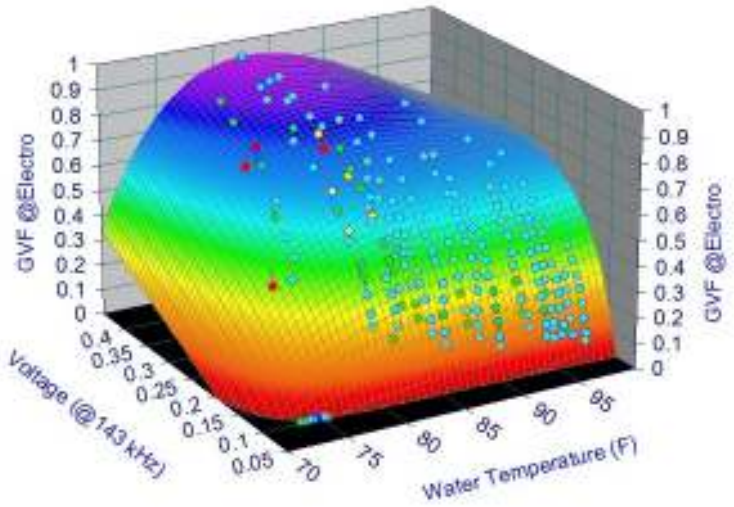

Figure7. 34 L11-R10 calibration curve at 143 KHz

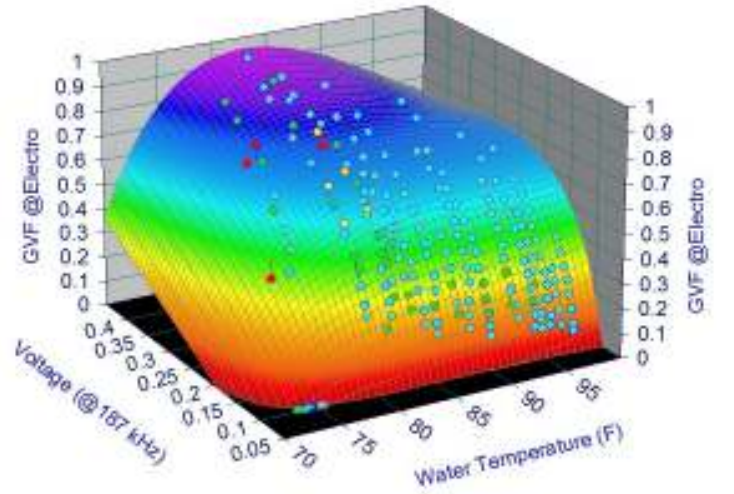

Figure7. 35 L11-R10 calibration curve at 187 KHz

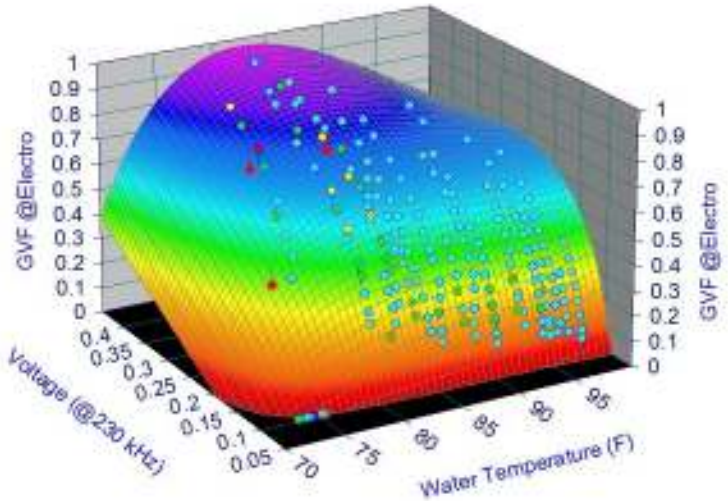

Figure7. 36 L11-R10 calibration curve at 230 KHz

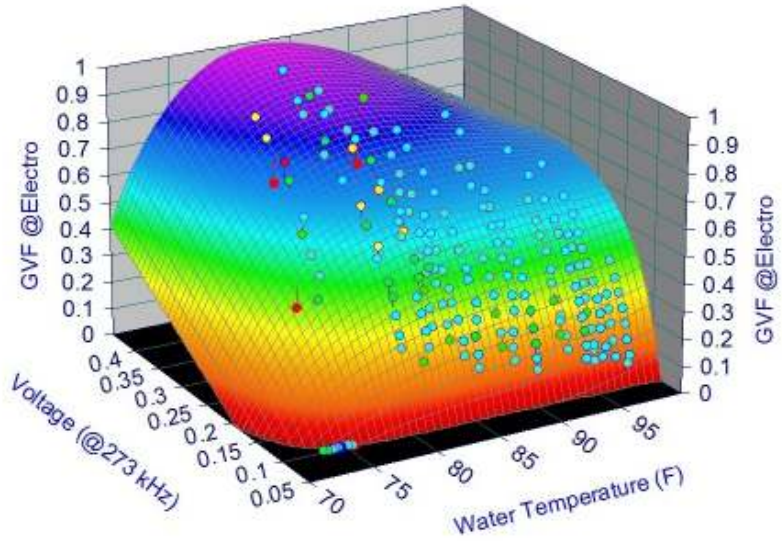

Figure7. 37 L11-R10 calibration curve at 273 KHz

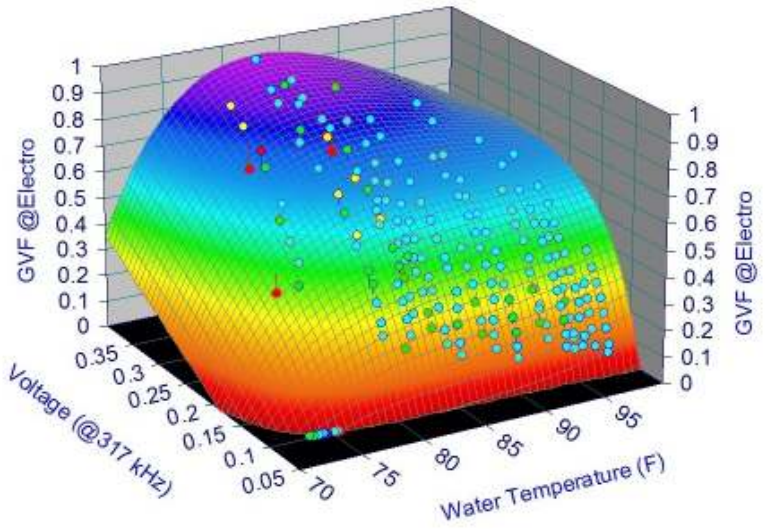

Figure7. 38 L11-R10 calibration curve at 317 KHz

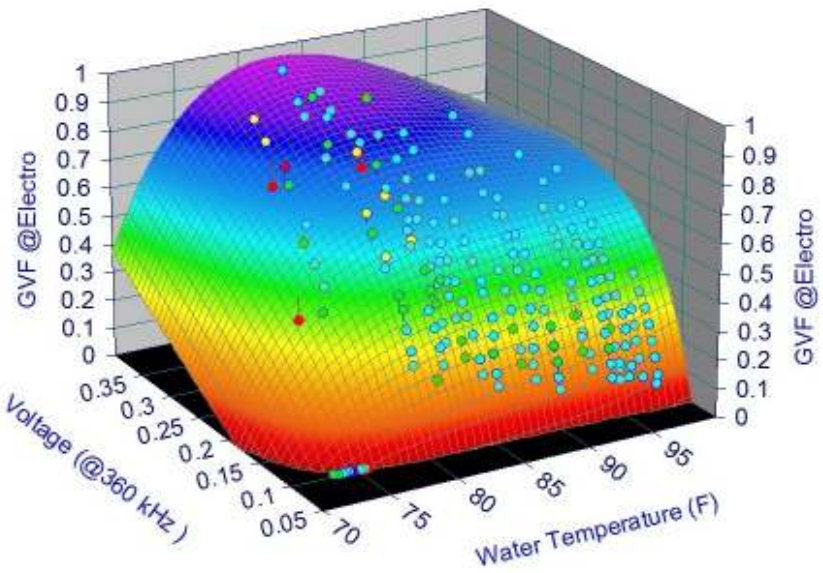

Figure7. 39 L11-R10 calibration curve at 360 KHz

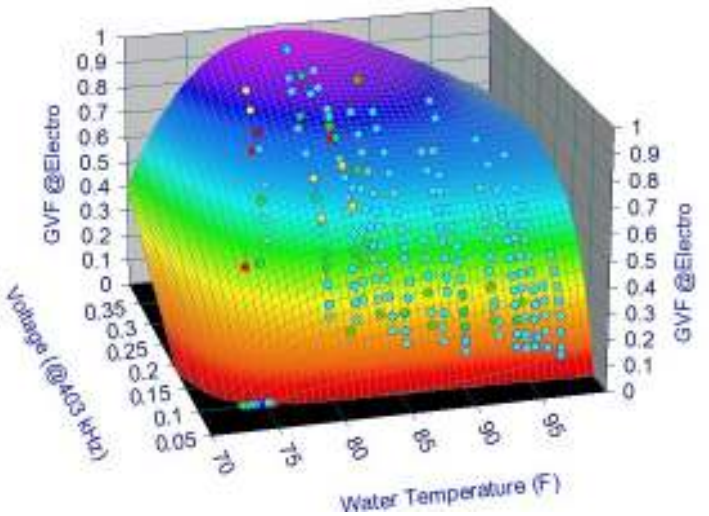

Figure7. 40 L11-R10 calibration curve at 403 KHz

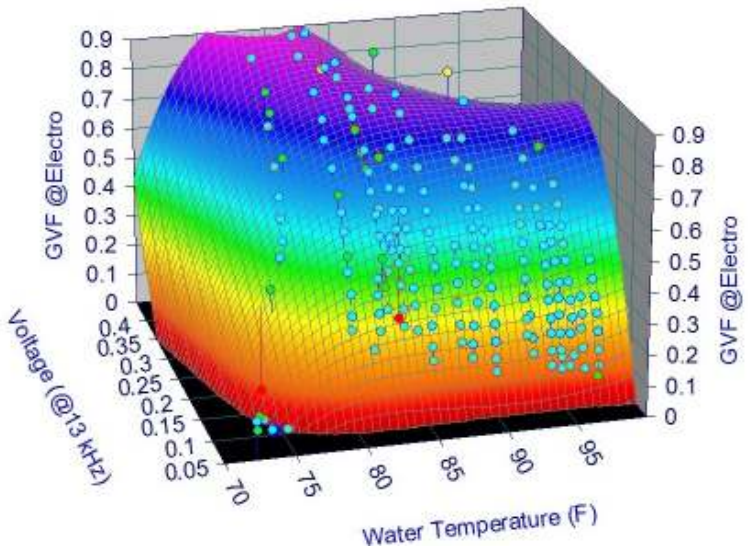

Figure7. 41 L11-R11 calibration curve at 13 KHz

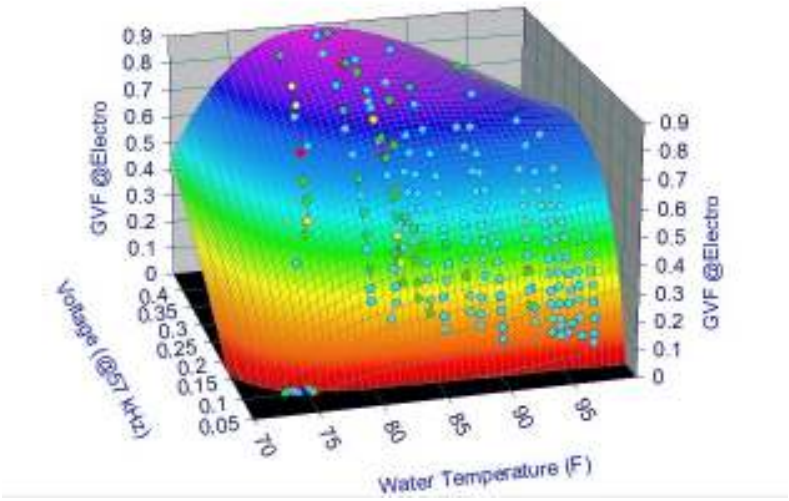

Figure7. 42 L11-R11 calibration curve at 57 KHz

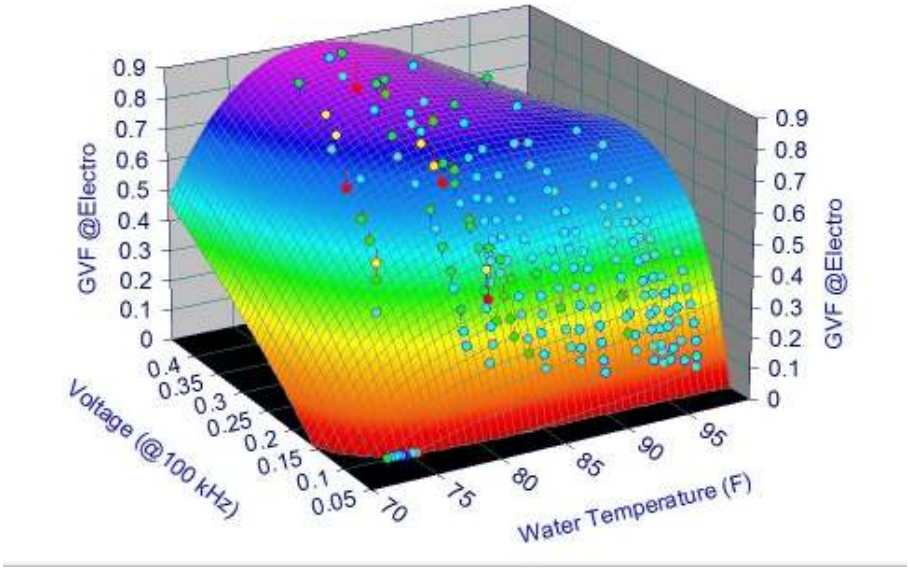

Figure7. 43 L11-R11 calibration curve at 100 KHz

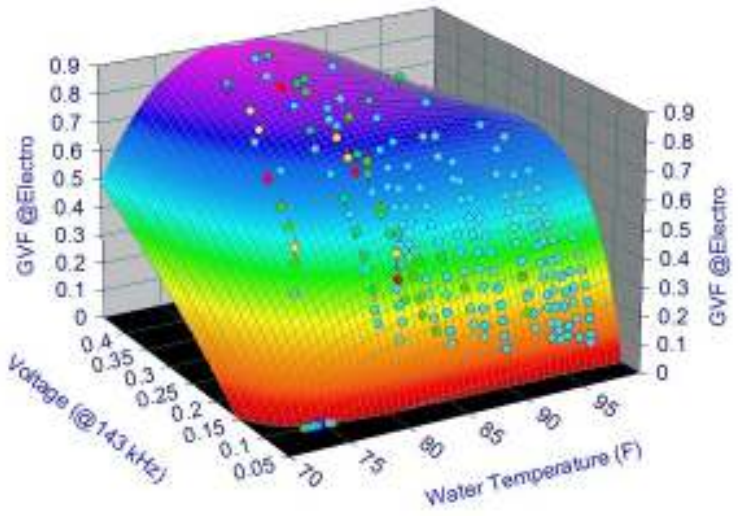

Figure7. 44 L11-R11 calibration curve at 143 KHz

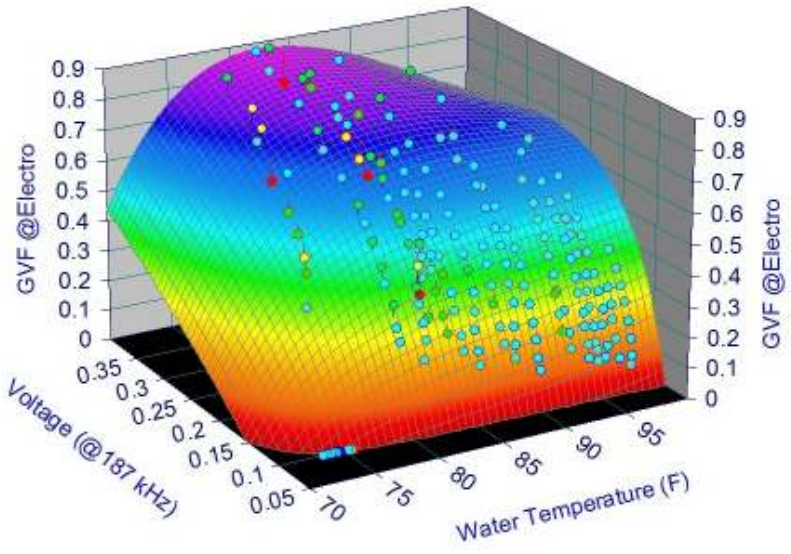

Figure7. 45 L11-R11 calibration curve at 187 KHz

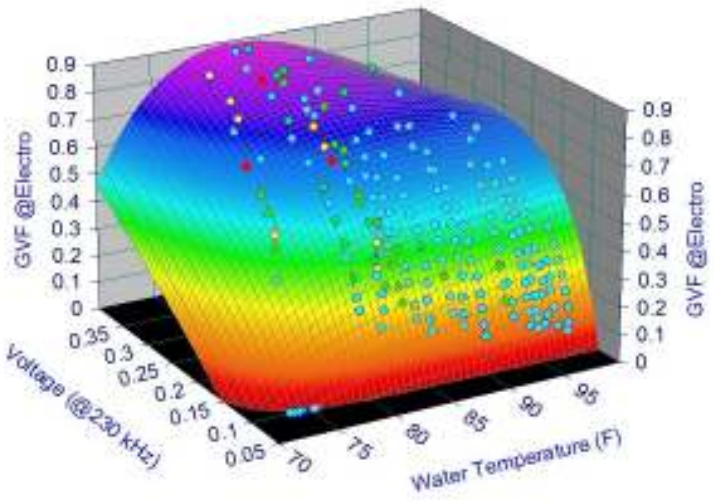

Figure7. 46 L11-R11 calibration curve at 230 KHz

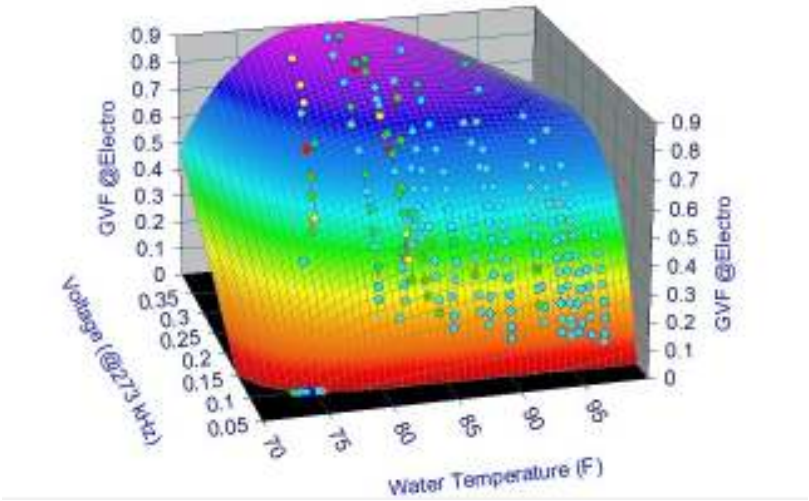

Figure7. 47 L11-R11 calibration curve at 273 KHz

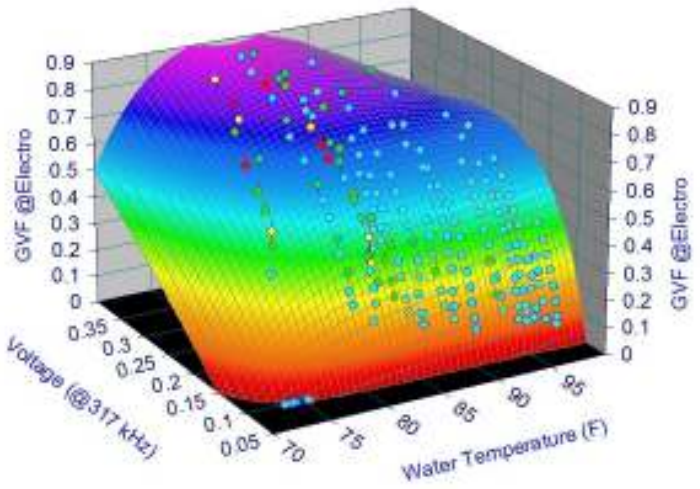

Figure7. 48 L11-R11 calibration curve at 317 KHz

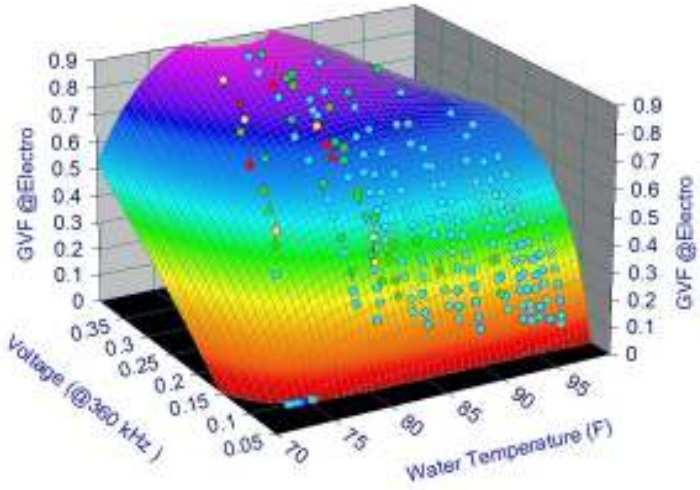

Figure7. 49 L11-R11 calibration curve at 360 KHz

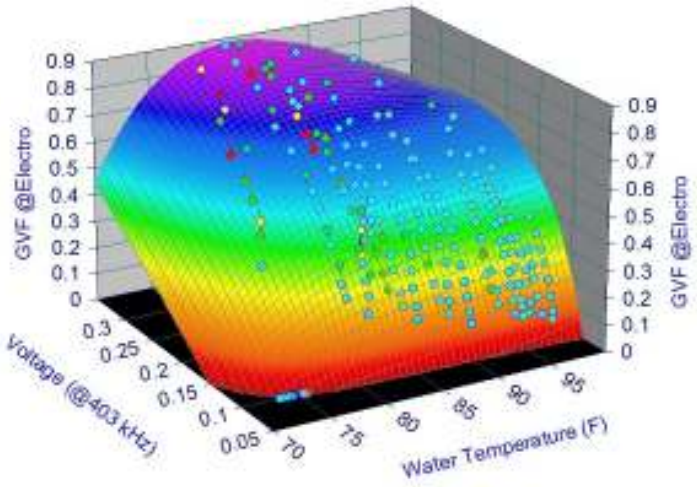

Figure7. 50 L11-R11 calibration curve at 403 KHz

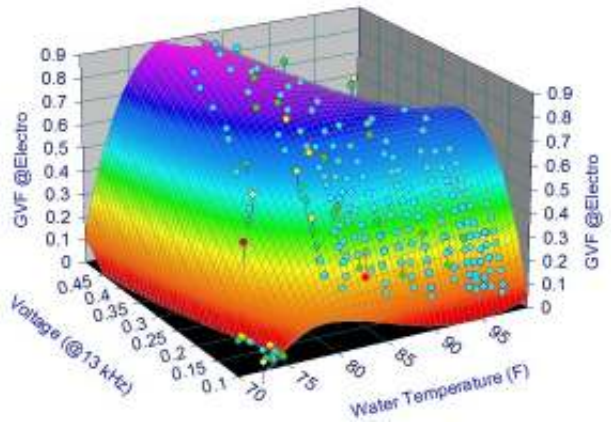

Figure7. 51 L11-R12 calibration curve at 13 KHz

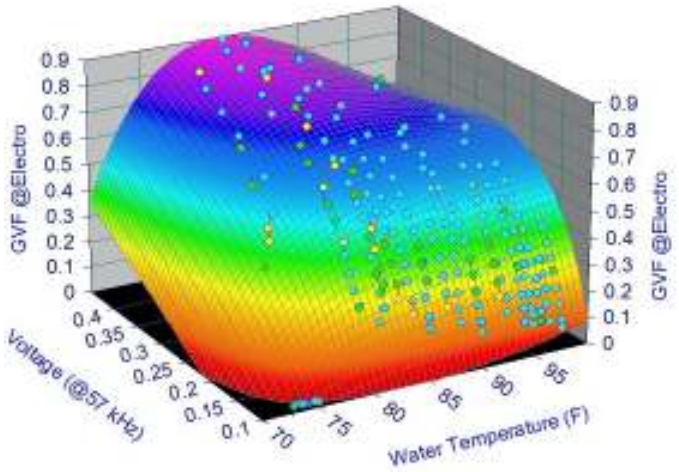

Figure7. 52 L11-R12 calibration curve at 57 KHz

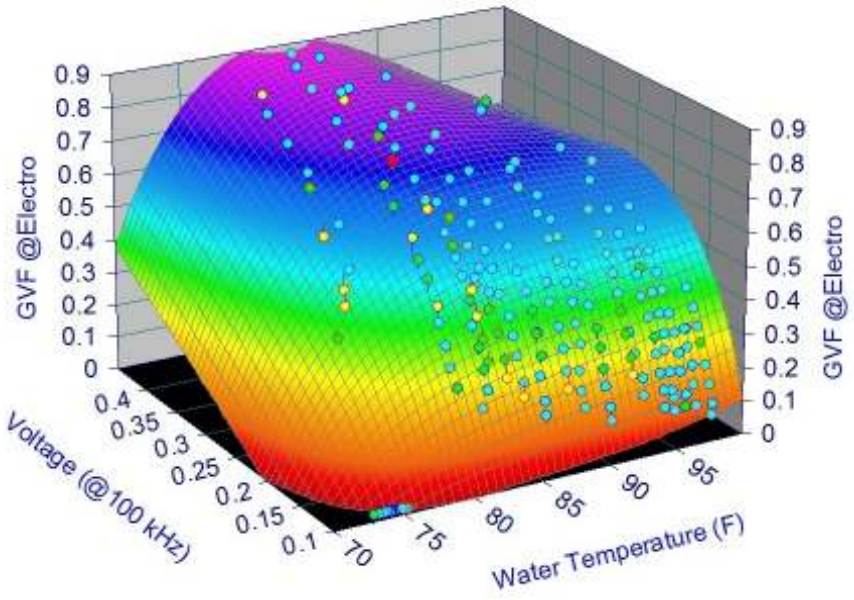

Figure7. 53 L11-R12 calibration curve at 100 KHz

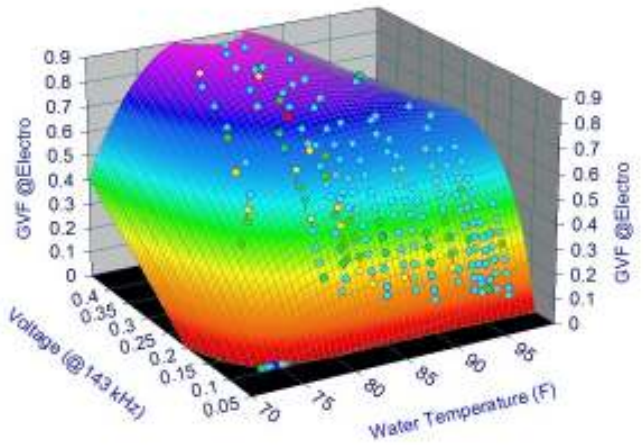

Figure7. 54 L11-R12 calibration curve at 143 KHz

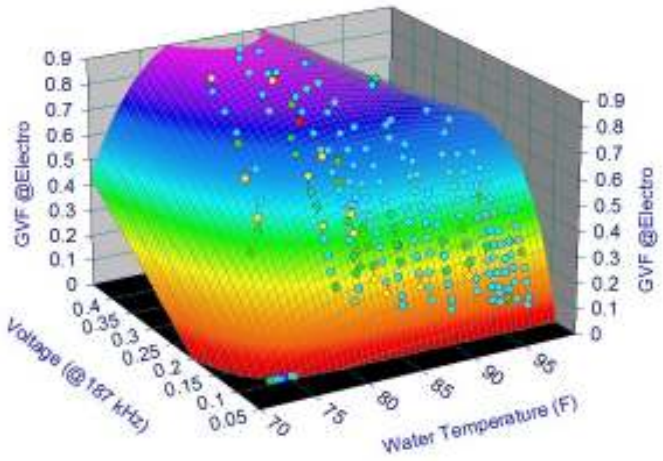

Figure7. 55 L11-R12 calibration curve at 187 KHz

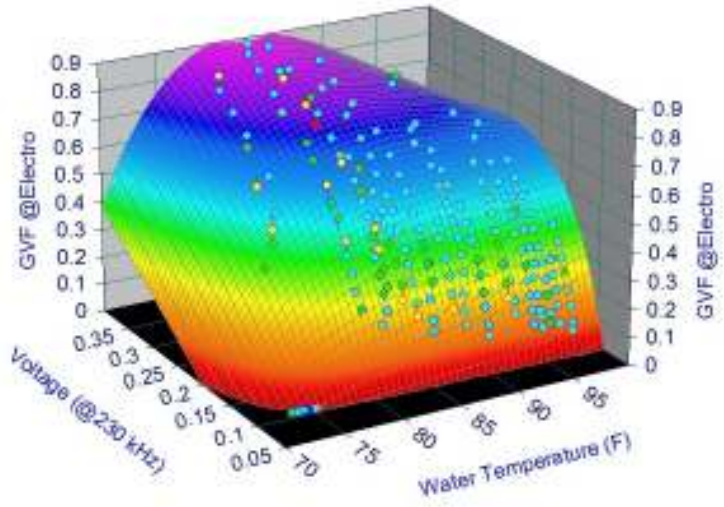

Figure7. 56 L11-R12 calibration curve at 230 KHz

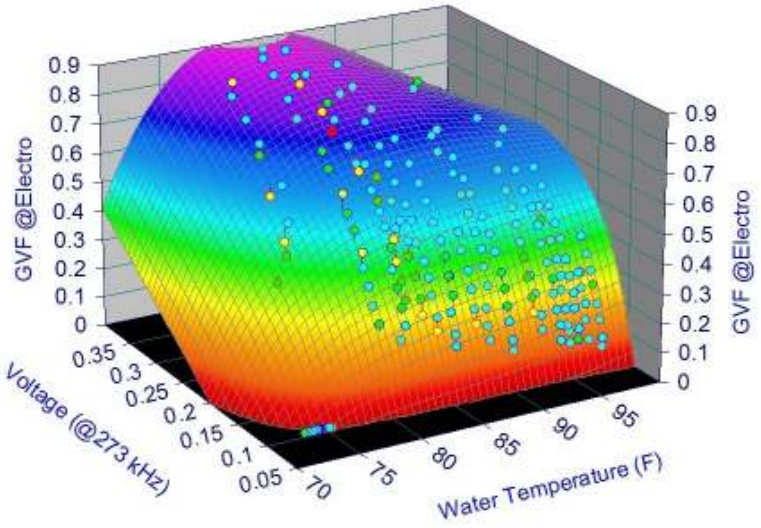

Figure7. 57 L11-R12 calibration curve at 273 KHz

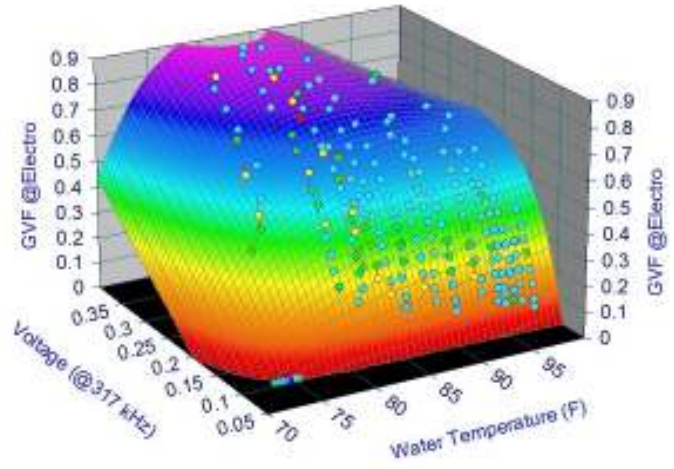

Figure7. 58 L11-R12 calibration curve at 317 KHz

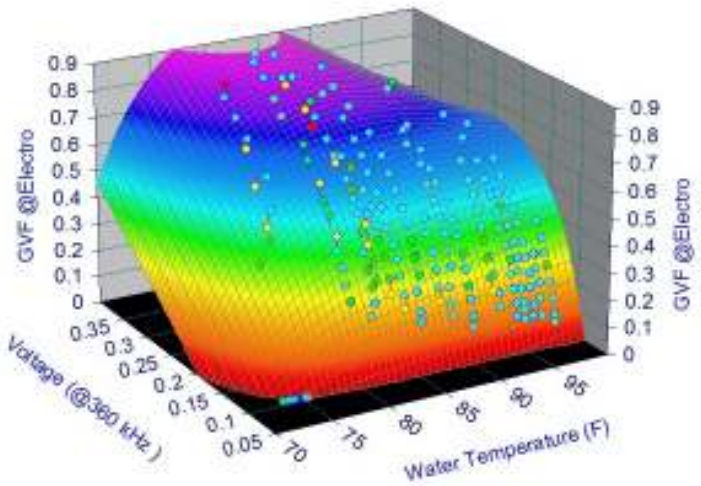

Figure7. 59 L11-R12 calibration curve at 360 KHz

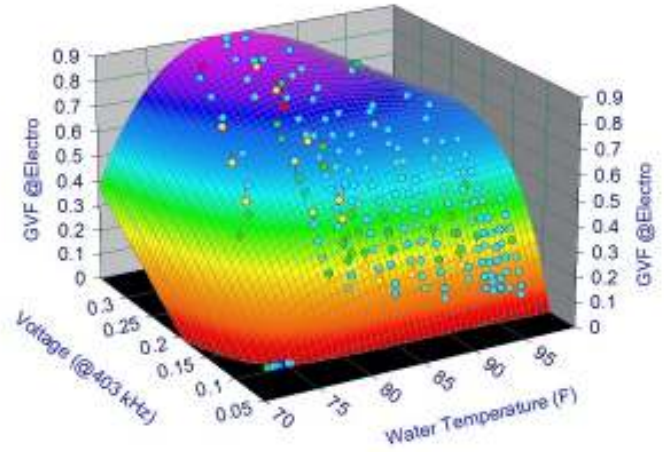

Figure7. 60 L11-R12 calibration curve at 403 KHz

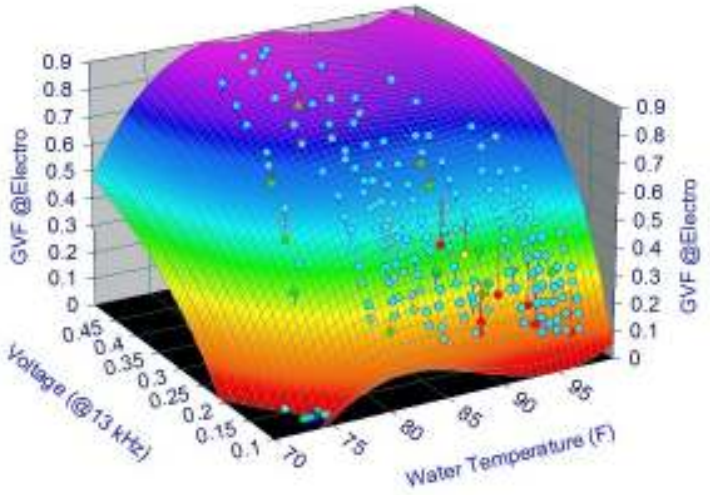

Figure7. 61 L12-R10 calibration curve at 13 KHz

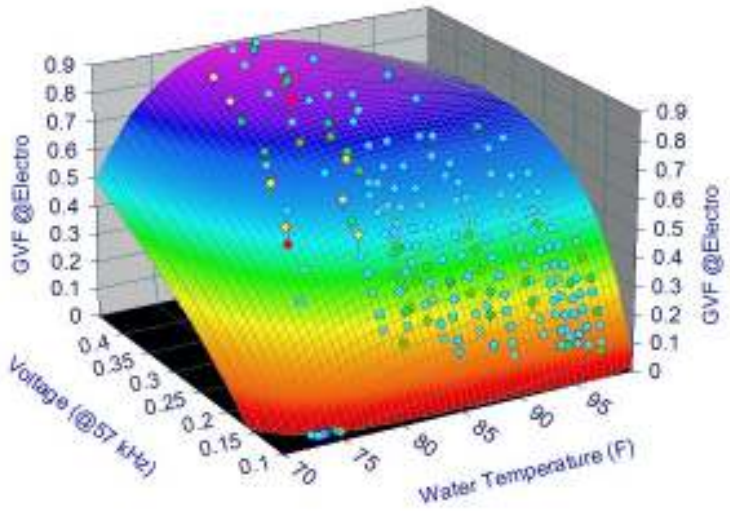

Figure7. 62 L12-R10 calibration curve at 57 KHz

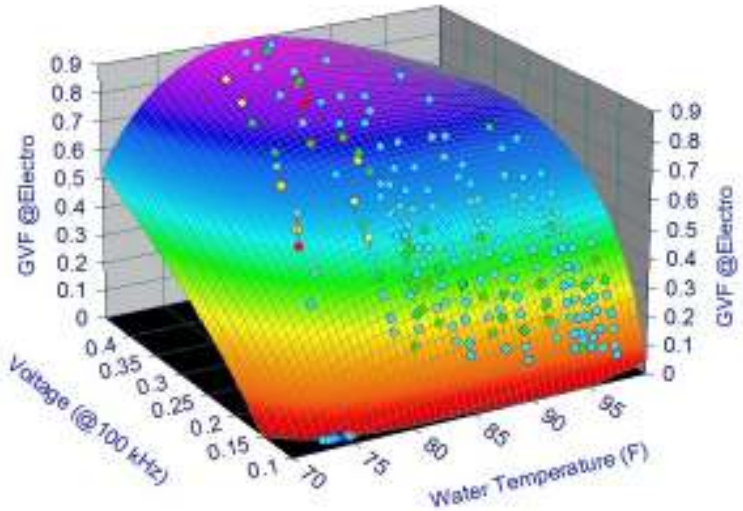

Figure7. 63 L12-R10 calibration curve at 100 KHz

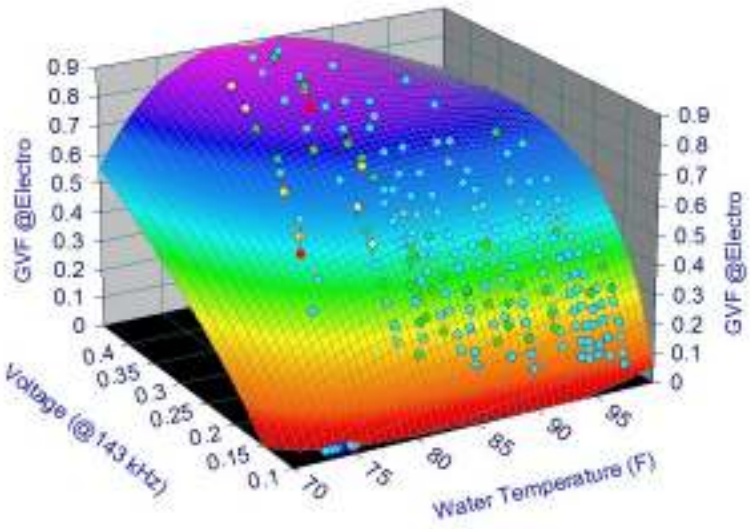

Figure7. 64 L12-R10 calibration curve at 143 KHz

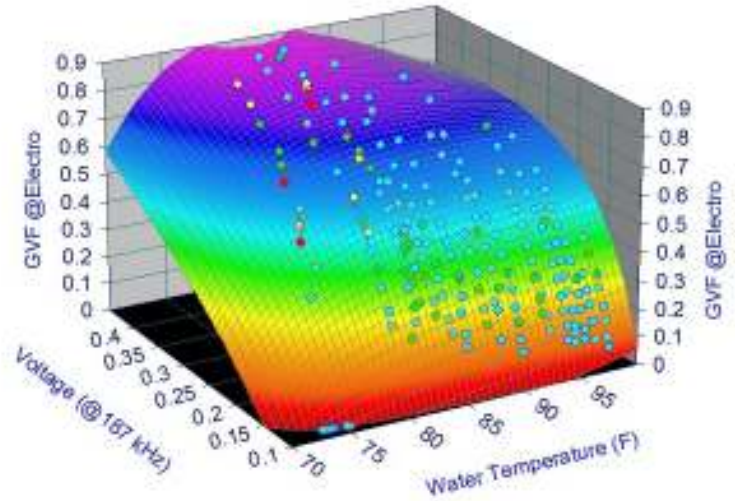

Figure7. 65 L12-R10 calibration curve at 187 KHz

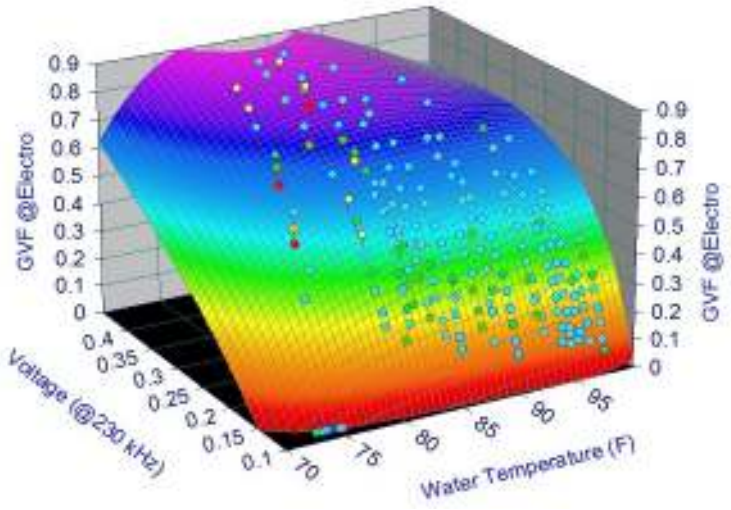

Figure7. 66 L12-R10 calibration curve at 230 KHz

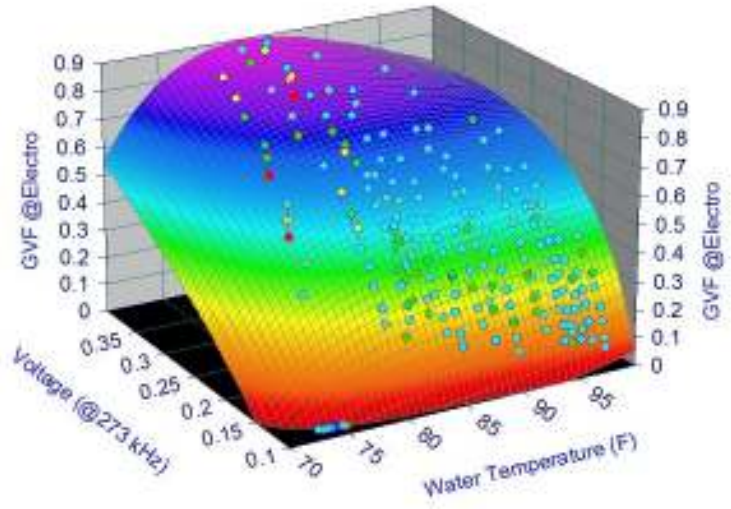

Figure7. 67 L12-R10 calibration curve at 273 KHz

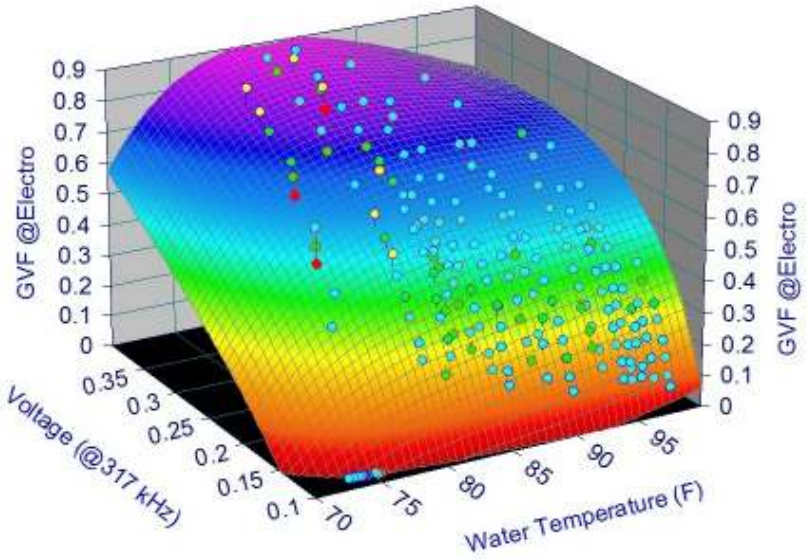

Figure7. 68 L12-R10 calibration curve at 317 KHz

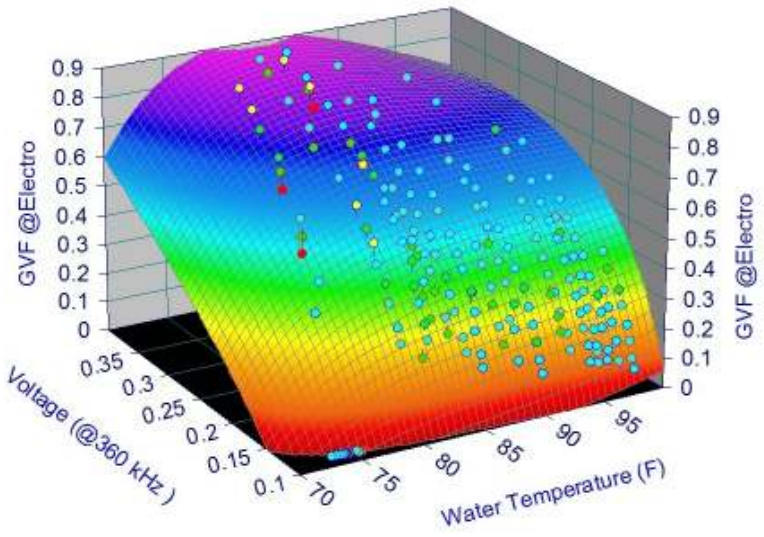

Figure7. 69 L12-R10 calibration curve at 360 KHz

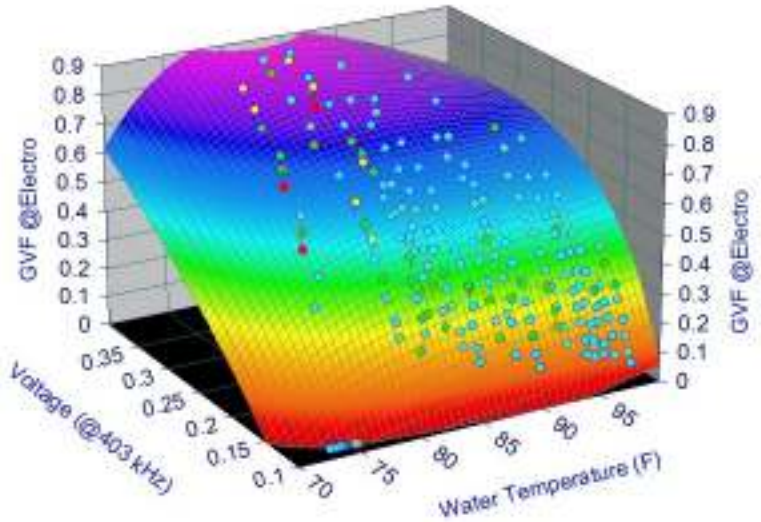

Figure7. 70 L12-R10 calibration curve at 403 KHz

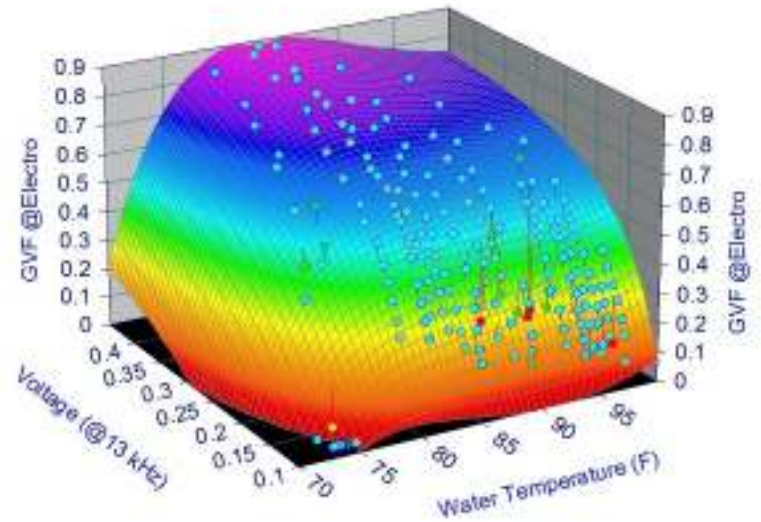

Figure7. 71 L12-R11 calibration curve at 13 KHz

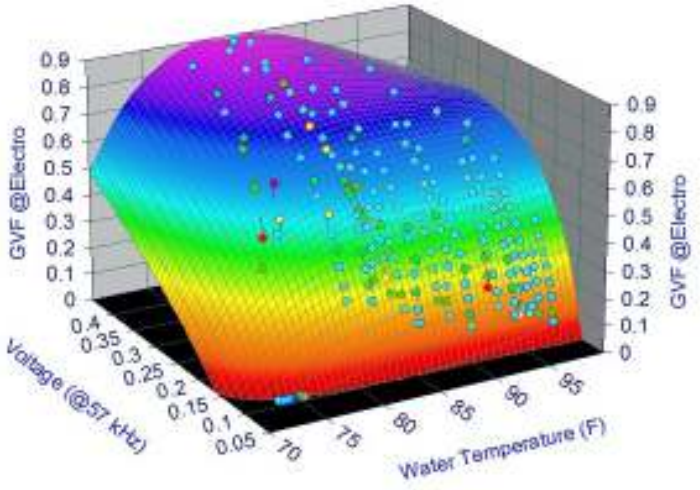

Figure7. 72 L12-R11 calibration curve at 57 KHz

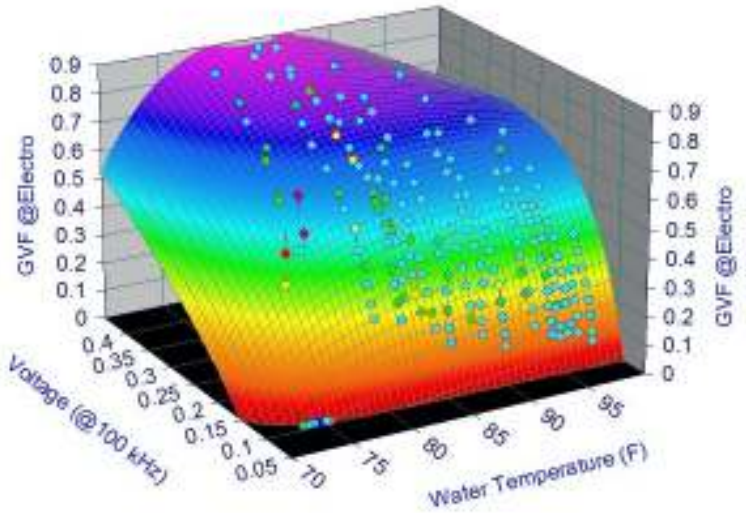

Figure7. 73 L12-R11 calibration curve at 100 KHz

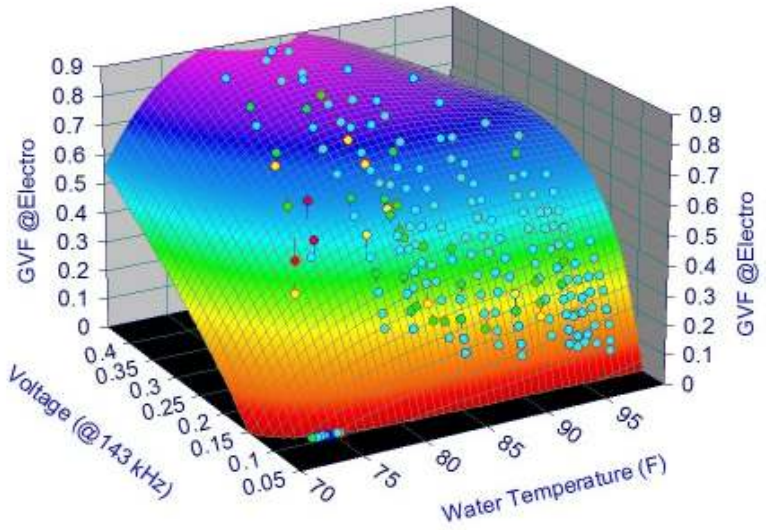

Figure7. 74 L12-R11 calibration curve at 143 KHz

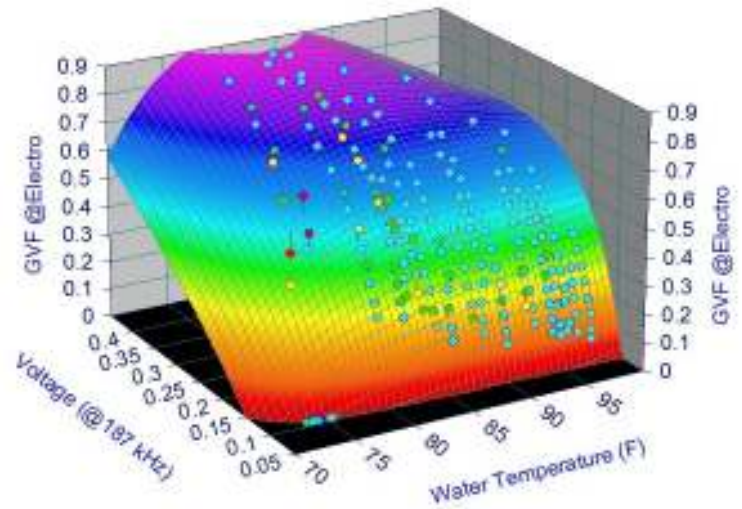

Figure7. 75 L12-R11 calibration curve at 187 KHz

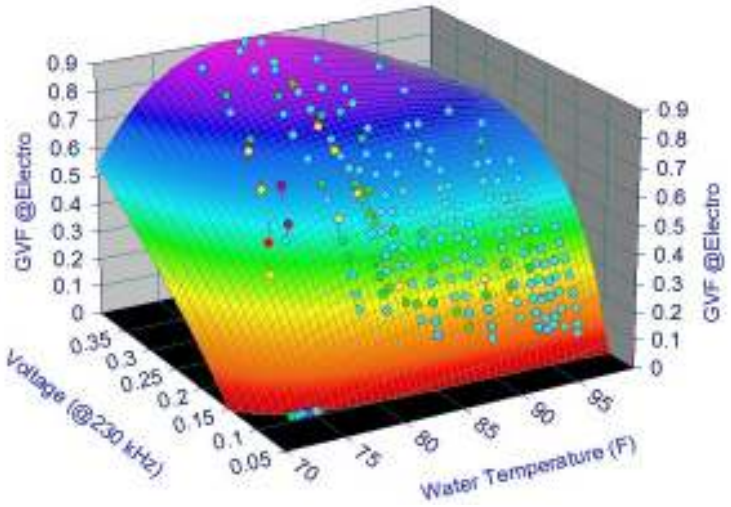

Figure7. 76 L12-R11 calibration curve at 230 KHz

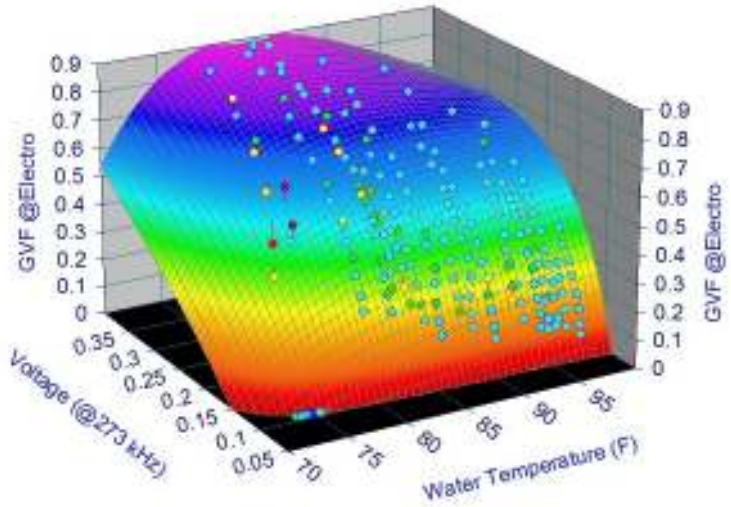

Figure7. 77 L12-R11 calibration curve at 273 KHz

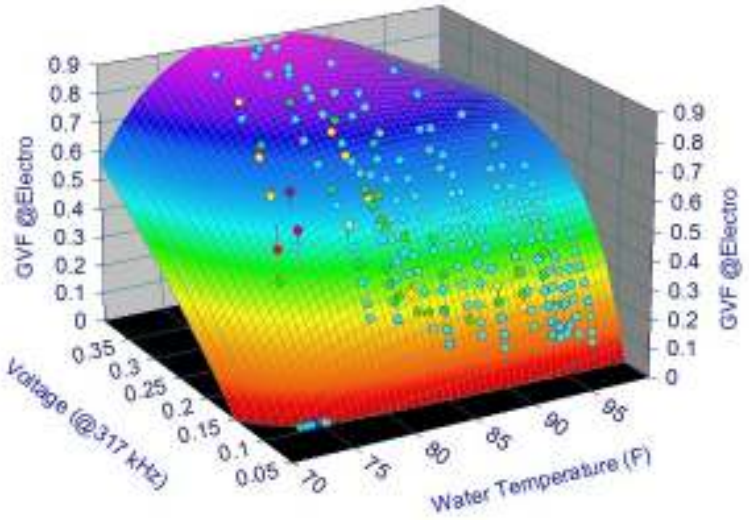

Figure7. 78 L12-R11 calibration curve at 317 KHz

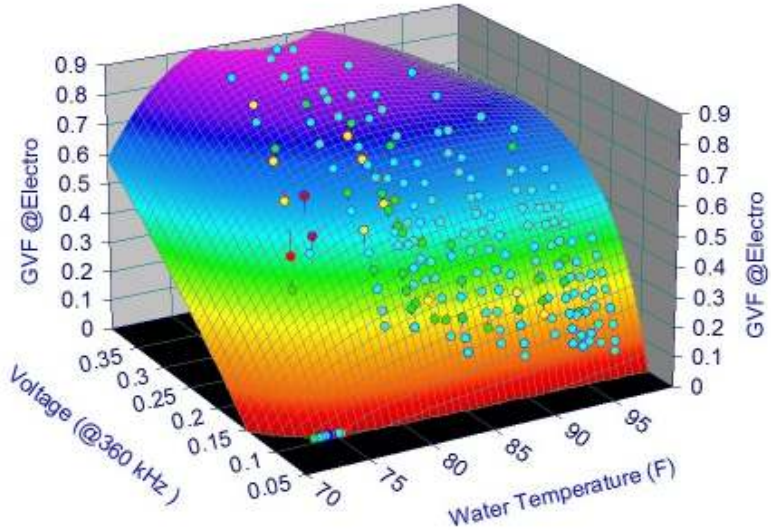

Figure 79 L12-R11 calibration curve at 360 KHz

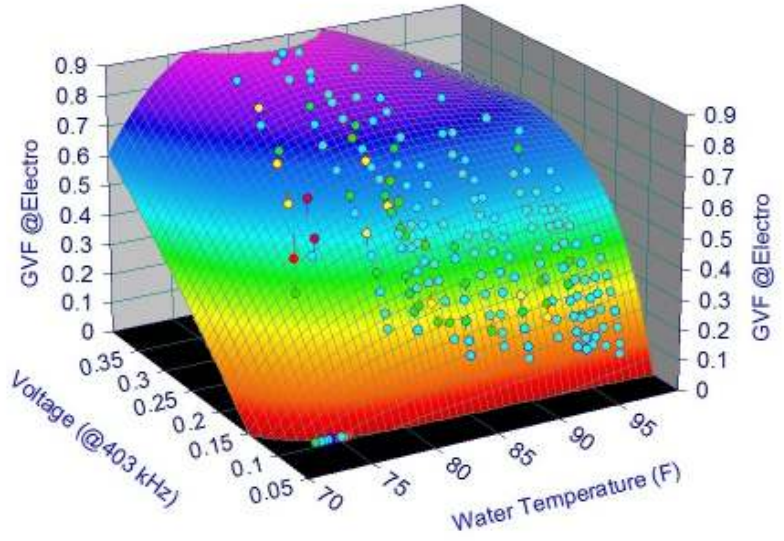

Figure7. 80 L12-R11 calibration curve at 403 KHz

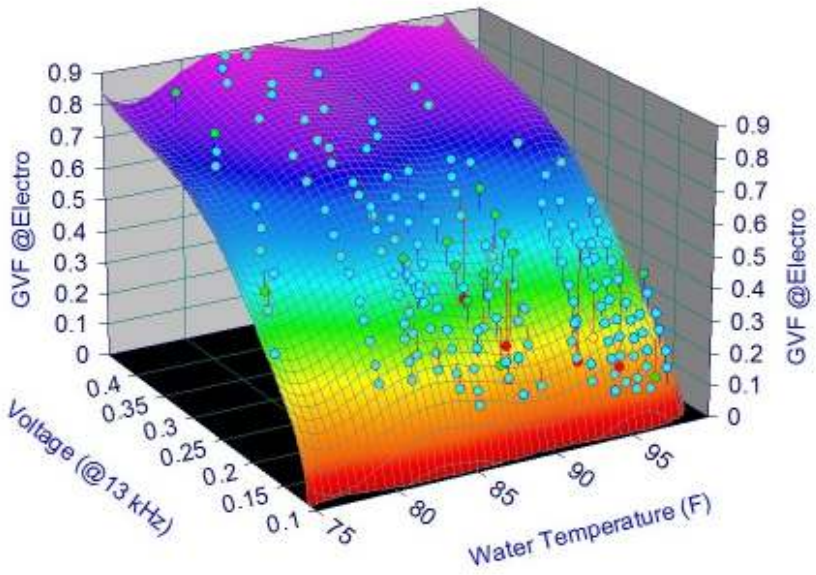

Figure7. 81 L12-R12 calibration curve at 13 KHz

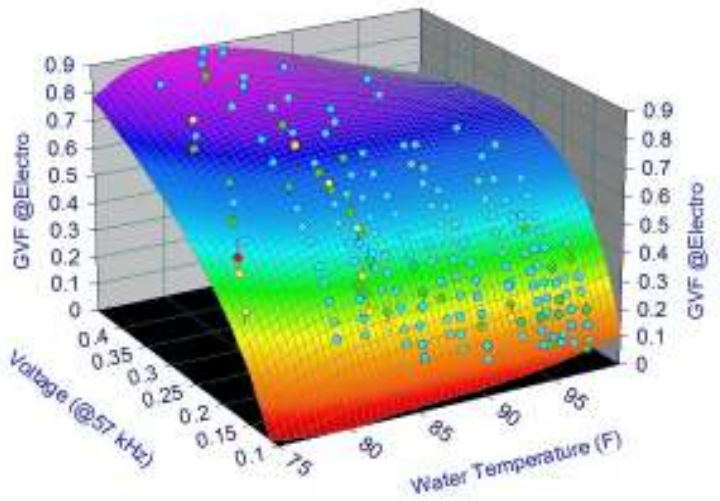

Figure7. 82 L12-R12 calibration curve at 57 KHz

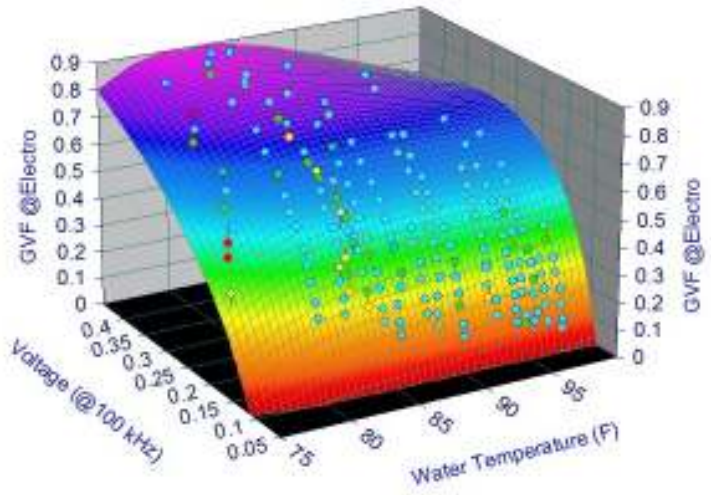

Figure7. 83 L12-R12 calibration curve at 100 KHz

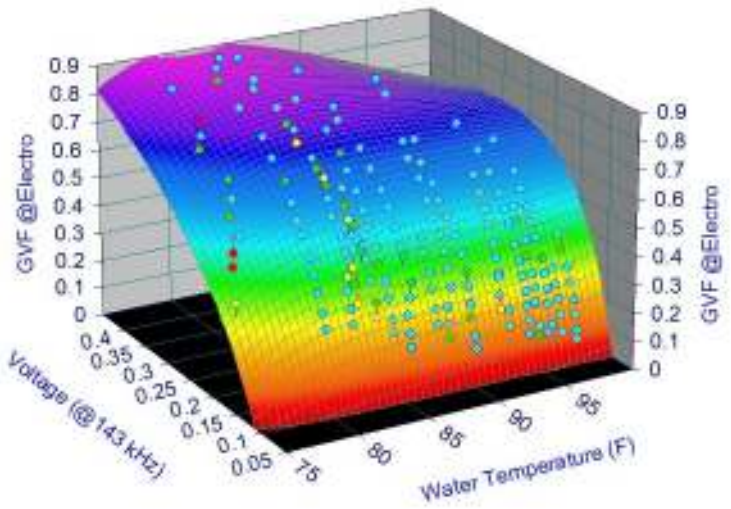

Figure7. 84 L12-R12 calibration curve at 143 KHz

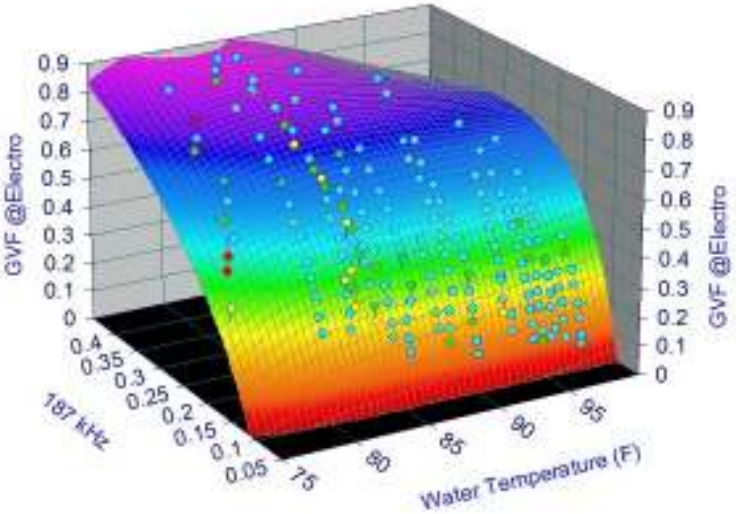

Figure7. 85 L12-R12 calibration curve at 187 KHz

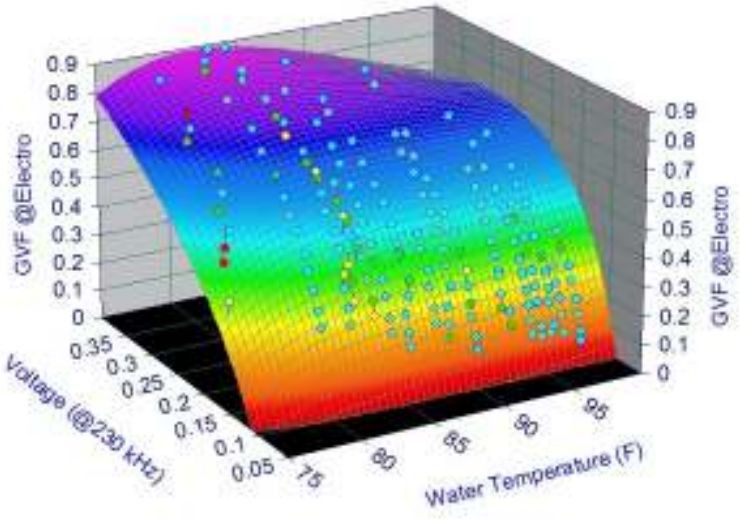

Figure7. 86 L12-R12 calibration curve at 230 KHz

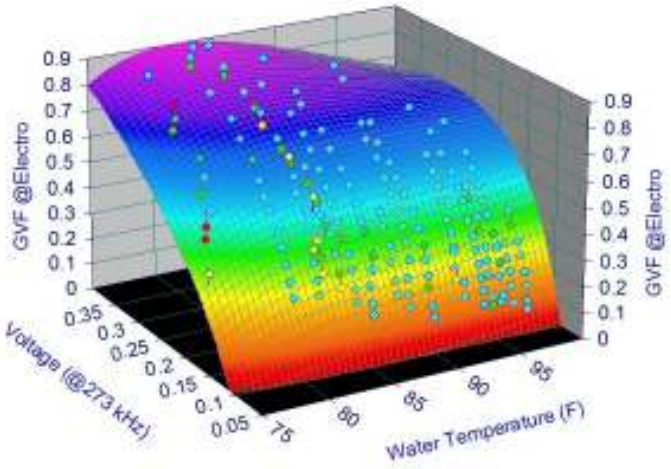

Figure7. 87 L12-R12 calibration curve at 273 KHz

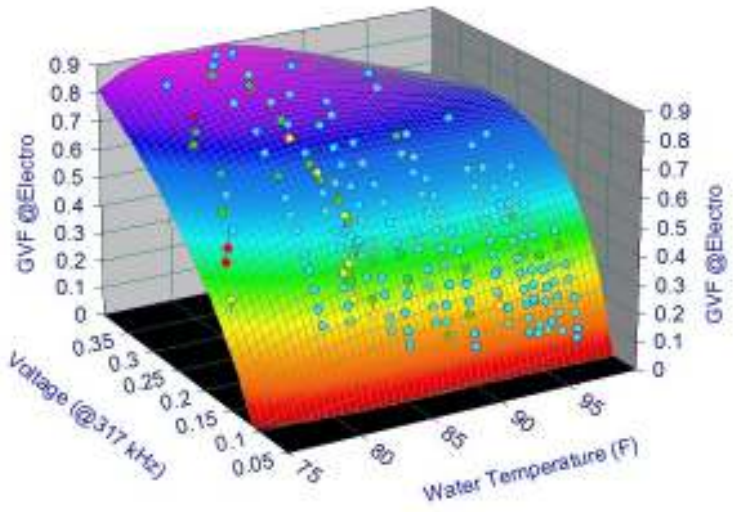

Figure7. 88 L12-R12 calibration curve at 317 KHz

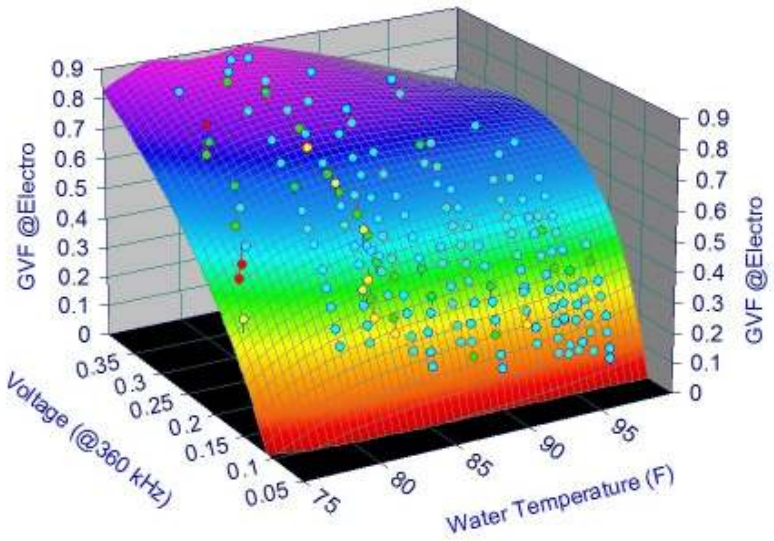

Figure7. 89 L12-R12 calibration curve at 360 KHz

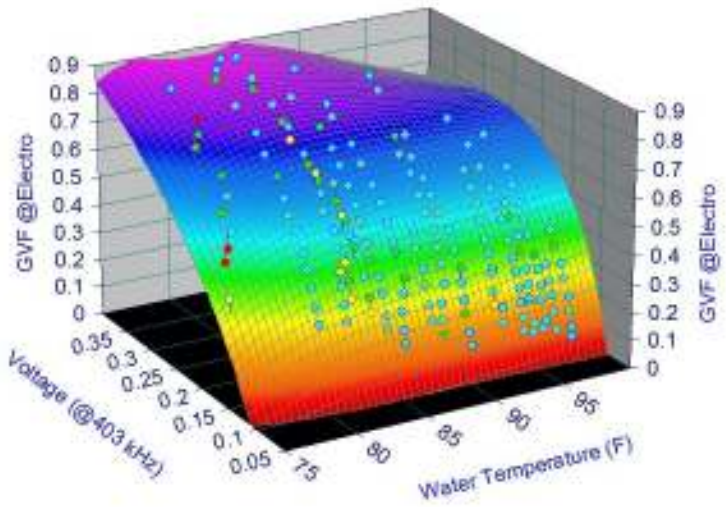

Figure7. 90 L12-R12 calibration curve at 403 KHz

APPENDIX B

NOMENCLATURE

A	Cross-Sectional Area
B	Beta ratio
D	Diameter
DP	Pressure Drop
F	Frequency
GVF	Gas Volume Fraction
KY	Calibration Coefficient
$\dot{m}$	Mass Flow rate
P	Pressure
R	Gas Constant
Re	Reynolds Number
ρ_g	Gas Density
ρ_l	Liquid Density
T	Temperature
U_g	Gas Velocity
Q	Quality
V	Voltage
Y	Expansion Factor

APPENDIX C

THE DRWAING OF ELECTRICAL IMPEDANCE PROBE